The [2Fe-2S] cluster of mitochondrial outer membrane protein mitoNEET has an O2-regulated nitric oxide access tunnel

Hoang, Thao Nghi; Wu-Lu, Meritxell; Collauto, Alberto; Hagedoorn, Peter Leon; Alexandru, Madalina; Henschel, Maike; Kordasti, Shahram; Mroginski, Maria Andrea; Roessler, Maxie M.; Ebrahimi, Kourosh H.

DOI
10.1002/1873-3468.15097

Publication date
2025

Document Version
Final published version

Published in
FEBS Letters

FEBS Letters

FEBS PRESS science publishing by scientists

RESEARCH ARTICLE

The [2Fe-2S] cluster of mitochondrial outer membrane protein mitoNEET has an O_2-regulated nitric oxide access tunnel

Thao Nghi Hoang[1,2], Meritxell Wu-Lu[3], Alberto Collauto[4], Peter-Leon Hagedoorn[5], Madalina Alexandru[1,6], Maike Henschel[1,6], Shahram Kordasti[6], Maria Andrea Mroginski[3], Maxie M. Roessler[4] and Kourosh H. Ebrahimi[1]

1 Institute of Pharmaceutical Science, King's College London, UK
2 Department of Pharmacy, Da Nang University of Medical Technology and Pharmacy, Vietnam
3 Department of Chemistry, Technical University of Berlin, Germany
4 Department of Chemistry and Centre for Pulse EPR Spectroscopy (PEPR), Imperial College London, UK
5 Department of Biotechnology, Delft University of Technology, TU Delft, The Netherlands
6 Comprehensive Cancer Center, King's College London, UK

Correspondence
K. H. Ebrahimi, School of Cancer & Pharmaceutical Sciences, Institute of Pharmaceutical Science, King's College London, Franklin-Wilkins Building, 150 Stamford Street, London SE1 9NH, UK
Tel: +44 207 848 4834
E-mail: kourosh.ebrahimi@kcl.ac.uk

(Received 11 December 2024, accepted 16 December 2024, available online 6 January 2025)

doi:10.1002/1873-3468.15097

Edited by Peter Brzezinski

The mitochondrial outer membrane iron–sulphur ([Fe-S]) protein mitoNEET has been extensively studied as a target of the anti-inflammatory and type-2 diabetes drug pioglitazone and as a protein affecting mitochondrial respiratory rate. Despite these extensive past studies, its molecular function has yet to be discovered. Here, we applied an interdisciplinary approach and discovered an explicit nitric oxide (NO) access site to the mitoNEET [2Fe-2S] cluster. We found that O_2 and pioglitazone block NO access to the cluster, suggesting a molecular function for the mitoNEET [2Fe-2S] cluster in mitochondrial signal transduction. Our discovery hints at a new pathway *via* which mitochondria can sense hypoxia through O_2 protection of the mitoNEET [2Fe-2S] cluster, a new paradigm in understanding the importance of [Fe-S] clusters for gasotransmitter signal transduction in eukaryotes.

Keywords: gasotransmitter; H_2S; hypoxia; iron–sulphur cluster; mitoNEET; nitric oxide

Proteins containing bioinorganic iron–sulphur ([Fe-S]) clusters constitute a large structurally and genetically diverse family and have functioned in many cellular processes since the emergence of life on Earth [1]. The [Fe-S] clusters in these proteins are synthesized using a complex machinery consisting of mitochondrial and cytoplasmic components in eukaryotes [2,3]. This biogenesis machinery has its roots in early life before earth's oxygenation [4], highlighting the importance of [Fe-S] clusters and proteins for all life forms. The clusters can have different stoichiometry of iron and sulphur and deviate in multiple ways from the classical all-cysteine pattern [5,6]. They play various functions [1]: electron transfer [7,8], catalysis [9], sulphur donor [10], sensors of reactive oxygen or nitrogen species [11–13] and structural stability [14]. In humans, two types of clusters, namely, [4Fe-4S](Cys)$_3$ and [2Fe-2S](Cys)$_3$(His) (Fig. 1A), are found in several [Fe-S] proteins playing vital roles in the immune response and mitochondrial function [1,15]. The [4Fe-4S](Cys)$_3$

Abbreviations
ddhCTP, 3′-Deoxy-3′,4′-didehydro-CTP; EPR, electron paramagnetic resonance; HYSCORE, hyperfine sublevel correlation; MeCN, acetonitrile; SAM, S-Adenosylmethionine; SAND, radical SAM-dependent nucleotide dehydratase; TZD, thiazolidinedione; VDAC, voltage-dependent anion channel; Viperin, virus inhibitory protein, endoplasmic reticulum associated, interferon inducible.

FEBS Letters **599** (2025) 952–970

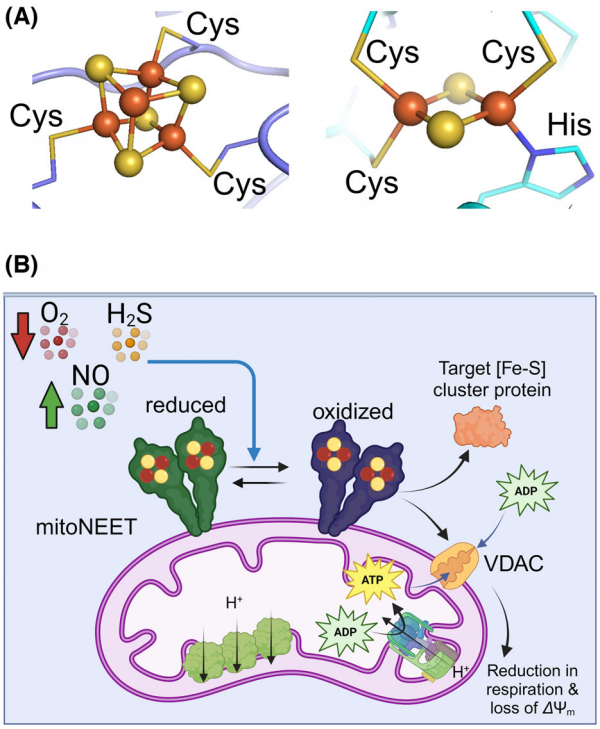

Fig. 1. The molecular mechanism of mitoNEET function is unknown. (A) The [4Fe-4S](Cys)$_3$ cluster of radical-SAM enzymes and the [2Fe-2S](Cys)$_3$(His) cluster of NEET family of proteins. (B) It is unknown if mitoNEET plays a specific role in sensing the levels of gasotransmitters NO and H_2S, as well as O_2 (blue arrow), and how this sensory function works. The expression of mitoNEET is associated with respiratory rate and mitochondrial function. Oxidized mitoNEET interacts with voltage-dependent anion channels, thereby reducing respiration rate and causing loss of mitochondrial membrane potential ($\Delta\Psi_m$). It is also shown that mitoNEET can transfer its cluster to the apo-client proteins.

cluster is present in the radical S-adenosylmethionine (SAM) enzymes [16]. These proteins have various cellular functions in humans [17]. The activity of some radical SAM enzymes such as the human SAND (hSAND) (radical SAM-dependent nucleotide dehydratase) [18,19] (also known as RSAD2, or viperin in humans) and Elp3 (the catalytic subunit of elongator complex) is associated with the innate immune response function [1] or oncogene expression and oncometabolism [20]. The [2Fe-2S](Cys)$_3$(His) cluster, on the other hand, is found in members of NEET (Asn-Glu-Glu-Thr) family of proteins, encoded by three genes CISD1 (encoding mitoNEET), CISD2 and CISD3 [21]. Among the proteins encoded by these genes, mitoNEET is localized at the mitochondrial outer membrane and is a target of the anti-inflammatory and type-2 diabetes drug pioglitazone (a class of thiazolidinedione (TZD) compounds) [22]. This protein regulates mitochondrial function and respiratory rate [23,24]. MitoNEET expression is associated with mitochondrial dysfunction in pathophysiological conditions like cancer, diabetes, age-related heart failure and neurodegeneration, highlighting mitoNEET as an effective drug target [22,25–30]. Pioglitazone targets mitoNEET to attenuate mitochondrial oxidative damage [22]. Additionally, the oxidized mitoNEET can transfer the [2Fe-2S] cluster to an apo-client protein, playing a role in the repair of target cytosolic [Fe-S] proteins [21,31,32]. The mitoNEET [2Fe-2S] cluster is shown to be pH sensitive [33,34] and react with O_2, H_2O_2 or nitric oxide (NO) [31–40]. Despite these extensive past studies and the established link between mitoNEET and mitochondrial activity and respiratory rate, the molecular mechanism of mitoNEET function is not fully understood. It is unknown how NO, O_2 or H_2O_2 access the cluster and react with it. We proposed that a redox imbalance changes the equilibrium between the reduced and oxidized mitoNEET, thereby altering mitochondrial respiration rate and activity (Fig. 1B) [20]. The redox imbalance in the cell could be associated with a decrease in O_2 level (hypoxia), an increase in NO production and a change in hydrogen sulphide (H_2S) level. These changes are shown to affect mitochondrial activity and function [41–44]. However, it is unknown how a change in the O_2 level will affect mitoNEET reaction with gasotransmitters NO or H_2S.

Here, we applied a multidisciplinary approach to study how gasotransmitter NO accesses the mitoNEET [2Fe-2S] cluster and elucidate a possible role of O_2 in this process. We studied the individual reaction of NO and H_2S with the mitoNEET cluster in the presence or absence of O_2. We discovered an explicit NO access site of the [2Fe-2S] cluster and found that O_2 or pioglitazone blocked NO access to the mitoNEET [2Fe-2S] cluster. We found that the reaction of NO with the cluster desensitized the cluster towards reduction by H_2S. Based on these findings and published data linking mitoNEET expression to mitochondrial activity, we postulate that the mitoNEET [2Fe-2S] cluster molecular function is to act as an O_2 and gasotransmitter sensor in hypoxia-associated mitochondrial signal transduction.

Materials and methods

Chemicals

All chemicals were reagent grade and purchased from ThemoFisher Scientific (Waltham, MA, USA), Fisher Scientific, (Loughborough, UK) or Merck, (Rahway, NJ, USA).

All anaerobic buffers were prepared a day prior to the experiments and stored in the glovebox overnight to ensure complete removal of dioxygen. H_2S donor and NO donor reagents were JK-2 (lithium 2-(phenylphosphonothioylamino)-3-phenylpropanoate) and D-184 (diethylamine NONOate sodium salt hydrate or DEA NONOate) respectively.

Cloning, expression and purification of mitoNEET

The *Escherichia coli* codon optimised gene-encoding soluble form of human mitoNEET (lacking 34 residues at the hydrophobic N-terminus), and its variants V70W and V70C were purchased from GeneArt (ThermoFisher). The synthetic gene for the soluble wild-type mitoNEET was in pMQ plasmid and ampicillin resistance. This synthetic gene had a 5′ and 3′ restriction site for KpnI and NcoI, respectively. The codon-optimized DNA sequence of soluble wild-type mitoNEET (without restriction sites) is described below. Additionally, the amino acid sequence of soluble wild-type mitoNEET and its two variants before cloning into pBAD/His C vector are described.

DNA sequence of wild-type mitoNEET gene used to clone into pBAD: TATGTTAAAGATCATCGTAACAAA GCCATGATCAACCTGCATATCCAGAAAGATAATCC GAAAATCGTGCACGCCTTTGATATGGAAGATCTGG GTGATAAAGCAGTTTATTGTCGTTGTTGGCGCAGC AAAAAGTTTCCGTTTTGTGATGGTGCACATACCAA ACATAATGAAGAAACCGGTGATAATGTTGGTCCG CTGATCATCAAAAAGAAAGAAACCTAA.

Wild-type mitoNEET cloned into pBAD: YVKDHRN-KAMINLHIQKDNPKIVHAFDMEDLGDKAVYCRCW RSKKFPFCDGAHTKHNEETGDNVGPLIIKKKET.

mitoNEET-V1 (V70W) gene cloned into pBAD: YVKDHRNKAMINLHIQKDNPKIVHAFDMEDLGDK AWYCRCWRSKKFPFCDGAHTKHNEETGDNVGPLII KKKET.

mitoNEET-V2 (V70C) gene clone into pBAD: YVKD HRNKAMINLHIQKDNPKIVHAFDMEDLGDKACYCR CWRSKKFPFCDGAHTKHNEETGDNVGPLIIKKKET.

Subsequently, the gene encoding each protein was cloned into pBAD/His C (Invitrogen) vector using KpnI and NcoI restriction enzymes (New England Biolabs, Hitchin, UK). After cloning into the pBAD/His C vector, the sequence of the 6-histidine tag present in the pBAD vector will be added to the N-terminus of the protein. The wild-type soluble mitoNEET was cloned in the lab and the presence of the correct insert was confirmed using restriction enzyme double digestion. The variants were cloned into pBAD/His C vector by GeneArt (ThermoFisher). The *E. coli* TOP10 strain (Invitrogen) was transformed with the final expression construct. A glycerol stock of the final *E. coli* cell was prepared and stored at −80 °C freezer. The glycerol stock was used to prepare LB Agar (100 μM ampicillin) plates. A single colony was picked and added to 50-mL LB media, and the pre-culture was grown overnight at 37 °C in a shaker (225 r.p.m.). The next day, cells were inoculated into a 2-L flask containing 500-mL terrific broth (TB) medium. The culture was grown in a shaker (37 °C, 225 r.p.m.) to an OD@600 nm of 0.6. Subsequently, mitoNEET production was induced by the addition of 0.04%w/v arabinose (final concentration). After 8 h, cells were collected and were pelleted by centrifugation at 4696 x *g* at 20 °C for 20 min. The cell pellet was stored at −80 °C. The pellet was thawed for 30 min at room temperature. Then, cells were resuspended in lysis buffer (50 mM Tris pH 8.0, 300 mM NaCl, 2% Triton, 0.5 mM Dithiothreitol (DTT), 0.5 mM DNAse and 0.5 mM PMSF (phenylmethylsulphonyl fluoride)) with a ratio of 3 mL lysis buffer to 5 mL cells. The cell paste was vortexed, and lysozyme (1 $mg \cdot mL^{-1}$) was prepared in lysis buffer and added to the resuspended cells (1 : 10 V/V). Fully resuspended cells were lysed on ice using a Branson SFX 150 Sonifier (Emerson, Leicester, UK). The conditions were 30%, 10 cycles each 30 s on followed by 10 s off. Each time, 5 mL of resuspended cells were lysed to ensure homogenous lysis. The crude lysate was centrifuged at 4696 x *g* at 4 °C for 40 min to remove cell debris. The supernatant containing soluble proteins was retained and transferred to an anaerobic glovebox (Belle, Weymouth, UK) ($O_2 < 5$ ppm). Protein purification under anaerobic conditions was achieved using a gravity column (Thermo Scientific) packed with Ni^{2+} resin (Thermo Scientific). The following buffers were used: Equilibration buffer (50 mM Tris, 300 mM NaCl, 2% triton, 5 mM imidazole, pH 7.5); wash buffer (50 mM Tris, 300 mM NaCl, 2% triton, 0.5 mM DTT, 10 mM imidazole, pH 7.5) and elution buffer (50 mM Tris, 300 mM NaCl, 2% triton, 0.5 mM DTT, 800 mM imidazole, pH 7.5). After purification, PD10 desalting column (Cytiva, Marlborough, MA, USA) was used to exchange the buffer to 50 mM phosphate buffer (pH 7.0) containing 100 mM NaCl and remove imidazole, triton and DTT. The final purified protein was divided into aliquots of 1 mL, flash frozen in liquid nitrogen and stored at −80 °C. Protein purity was assessed by SDS/PAGE, and protein concentration was determined using the bicinchoninic acid (BCA) assay with bovine serum albumin as a standard. The concentration of mitoNEET was between 200 and 270 μM unless otherwise stated. Protein concentrations are the average of three independent measurements ±15% error.

Expression and purification of hSAND

The *E. coli* codon-optimized gene for expression of a soluble form of hSAND (lacking N-terminal hydrophobic domain) was cloned in pBAD/His-C plasmid, as explained previously [45]. *Escherichia coli* TOP10 cells were transformed with the plasmid encoding hSAND. Expression of hSAND was achieved, as explained for mitoNEET, by the addition of 0.04% W/v arabinose (final concentration). Eight hours after induction, cells were harvested using centrifugation at 4696 x *g* at 20 °C for 20 min. The cell pellet

was stored at −80 °C. Cell lysis was performed as explained for mitoNEET. The cell lysate was transferred to an anaerobic glovebox (Belle Technologies) and added to centrifuge tubes. Cell debris was removed by centrifugation at 7810 x *g* and 4 °C for 20 min under aerobic conditions. After centrifugation, the supernatant was retained and immediately transferred to the anaerobic glovebox ($O_2 < 5$ ppm). Anaerobic purification was achieved using a gravity column packed with Ni^{2+} resin (Thermo Scientific). The following buffers were used: Equilibration buffer (50 mM Tris, 300 mM NaCl, 2% triton and 5 mM imidazole, pH 7.5); wash buffer (50 mM Tris, 300 mM NaCl, 2% v/v triton, 0.5 mM DTT and 10 mM imidazole, pH 7.5); and elution buffer (50 mM Tris, 300 mM NaCl, 2% v/v triton, 0.5 mM DTT and 500 mM imidazole, pH 7.5). Subsequently, the PD10 desalting column was used to exchange the buffer and remove imidazole, triton and DTT. The final buffer was 50 mM MOPS (3-(Morpholin-4-yl)propane-1-sulfonic acid) buffer pH 7.0 containing 100 mM NaCl unless otherwise stated. The sample was flash frozen in liquid nitrogen and stored at −80 °C. The protein purity was confirmed by 10% SDS/PAGE gel, and the protein concentration was measured using the BCA assay. The concentration of hSAND was between 90 and 100 μM unless otherwise stated. Protein concentrations are the average of three independent measurements ±15% error.

Preparation of different reagents for oxidation/reduction reactions monitored by UV–visible spectrophotometry

To prepare the stock solution of sodium dithionite, NO donor, H_2S donor or pioglitazone, the desired amount (mg) of their corresponding salt was added to a 1.5-mL Eppendorf tube and transported into the glovebox. An aliquot of anaerobic buffer (50 mM phosphate buffer, pH 7.0, containing 100 mM NaCl) was added to each vial to reach the desired final concentration, determined based on a specific final reagent to protein and a known protein concentration. To prepare the H_2O_2 solution, 500 μL of H_2O_2 30%w/v (Fisher) was transferred into the glovebox *via* a 1.5-μL Eppendorf vial. The H_2O_2 solution was then diluted in anaerobic buffer (50 mM phosphate buffer, pH 7.0, containing 100 mM NaCl).

General experimental conditions

The proteins and reagent concentrations of samples are provided in the figure legend for each experiment. For all experiments (unless otherwise stated), the buffer was 50 mM phosphate buffer, pH 7.0 and contained 100 mM NaCl. Samples were prepared anaerobically ($O_2 < 5$ ppm) in a glovebox (Bele Technology, Weymouth, UK) at room temperature (22 °C) unless otherwise stated. After adding NO donor, H_2S donor or H_2O_2 to the mitoNEET or hSAND solution, samples were incubated for 4 h at room temperature (22 °C) under anaerobic conditions ($O_2 < 5$ ppm) in a glovebox (Bele Technology) before subsequent treatment or measurements. To expose mitoNEET or hSAND to O_2, the anaerobic solutions of the proteins were taken out of the glovebox and incubated under aerobic conditions at room temperature for 4 h. Subsequently, samples were used for further analysis unless otherwise stated. All samples were centrifuged before measurement to remove any possible precipitate interfering with measurement.

Exposure of proteins to NO or H_2S

To expose the reduced or oxidized hSAND or mitoNEET to NO or H_2S, the following components were added in order: 50 μL purified protein solution, phosphate buffer pH 7.0 (an aliquot was added to make up a final volume of 700 μL), 50 μL sodium dithionite (for reduced samples only) and 50 μL NO- or H_2S-donor solution. When sodium dithionite was added, samples were incubated for 15 min, and then NO- or H_2S-releasing molecules were added. The samples were incubated for 4 h in the glovebox under anaerobic conditions before analysis using UV–visible spectrophotometry. Five samples were prepared for the NO titration experiments. Initially, 50 μL purified protein solution and phosphate buffer pH 7.0 (an aliquot was added to make up a final volume of 700 μL) were mixed. Subsequently, NO donor (1.12 mM stock prepared in phosphate buffer) was added anaerobically to each sample in varying ratios relative to mitoNEET: 5, 10, 50, 100 or 500 μL, corresponding to a NO donor/mitoNEET ratio of 0, 0.5, 1, 5, 10 or 50 respectively. These samples were incubated anaerobically for 4 h before analysis using UV–visible spectrophotometry. Afterwards, all samples were immediately transferred into a glovebox and incubated overnight to eliminate residual NO. The following day, 50 μL of H_2S-donor solution was added to each sample, followed by another 4-h incubation under anaerobic conditions before UV–visible spectrophotometry analysis. All measurements were repeated two times to confirm reproducibility.

Exposure of proteins to H_2O_2

To expose the reduced or oxidized hSAND or mitoNEET to H_2O_2, the following components were added in order: 50 μL purified protein solution, phosphate buffer pH 7.0 (an aliquot was added to make up a final volume of 700 μL), 50 μL sodium dithionite (for reduced samples only) and 50 μL diluted H_2O_2 solution. For the reduced sample after adding sodium dithionite, samples were incubated at room temperature under anaerobic conditions for 30 min. In the case of mitoNEET, sodium dithionite was removed under anaerobic conditions ($O_2 < 5$ ppm) using a PD10 desalting column, and the formation of the reduced cluster was confirmed using UV–visible spectrophotometry. The samples were then

mixed well and incubated for 4 h in the glovebox before analysis using UV–visible spectrophotometry.

Exposure of proteins to O_2

To expose oxidized mitoNEET or hSAND to molecular oxygen, the as-isolated protein was incubated for 4 h in atmospheric conditions. To expose reduced mitoNEET or hSAND to the molecular oxygen, an aliquot of isolated mitoNEET or hSAND was first transported into the anaerobic glovebox. A reaction was made by adding 50 μL purified protein solution, phosphate buffer pH 7.0 (an aliquot was added to make up a final volume of 700 μL) and 50 μL sodium dithionite. Subsequently, the reduced protein was incubated for 4 h under aerobic conditions at room temperature (22 °C), and samples were analysed using UV–visible spectrophotometry.

Sequential reduction–oxidation mitoNEET

To test the oxidation with NO, H_2O_2 or O_2, and subsequent reduction by H_2S or sodium dithionite samples were prepared as follows. First, 50 μL of purified mitoNEET was diluted in an aliquot of phosphate buffer pH 7.0 (an aliquot was added to make up a final volume of 700 μL), followed by the addition of 50 μL NO-donor solution or H_2O_2 (NO donor or H_2O_2-to-mitoNEET ratio of 1). The samples were incubated overnight under anaerobic conditions at room temperature (22 °C) to ensure complete removal of any residual NO in the solution. For oxidation with O_2, as-isolated mitoNEET was taken out of the glovebox, and samples were retained under aerobic conditions at room temperature for 4 h. Subsequently, samples were transported back into the anaerobic glovebox and incubated overnight under anaerobic conditions to ensure the removal of any residual O_2. The next day, 50-μL H_2S-donor solution (to-mitoNEET ratio of 1) or sodium dithionite (to-mitoNEET ratio of 1) was added to each sample, and reactions were incubated under anaerobic conditions for 4 h. To reduce samples and then test oxidation, H_2S donor or $(S_2O_4)^{2-}$ was first added, and then O_2 or NO donor, and all the other conditions were kept the same. Samples were subject to analysis using UV–visible spectrophotometry before and after the addition of reducing and oxidizing agents. In all cases, the total final volume of the sample was 700 μL.

NO and O_2 competition studies

To test the competition between NO and O_2, we tested if H_2S could reduce the NO-exposed cluster in the presence of O_2 and compared that with the control in the absence of O_2. The control and sample were prepared in parallel. At first, for the control and sample, 50-μL purified protein solution was added to phosphate buffer pH 7.0 (an aliquot was added to make up a final volume of 700 μL) inside an aerobic glovebox ($O_2 < 5$ ppm). Subsequently, the reaction sample in a 1-mL cuvette was taken out of the anaerobic glovebox (Belle Technology) and left under aerobic conditions for 4 h with gentle shaking to allow slow diffusion of O_2. The control was incubated under anaerobic conditions ($O_2 < 5$ ppm) at the same time. After 4 h, 50 μL of DEA NONOate solution (NO donor) was added to the sample (under aerobic conditions) and control (under anaerobic conditions) to reach a mitoNEET/NO-donor ratio of 1. The sample and the control were incubated for 4 h under aerobic and anaerobic conditions, respectively. The sample was then transported back into the glovebox. The sample and control were incubated overnight to ensure the removal of any residual O_2 and NO. The next day, 50-μL H_2S-donor solution was added anaerobically in the glovebox ($O_2 < 5$ ppm) to the sample and control to reach a final mitoNEET/H_2S-donor ratio of 1. The sample and control were then incubated under anaerobic conditions for 4 h. At each stage, the sample and control were subject to analysis using UV–visible spectrophotometry. In all cases, the total final volume of the sample was 700 μL. Experiments were repeated at least three times on different days to confirm reproducibility.

Prediction of NO released by DEA NONOate

The measured decomposition rate constant (k_{dec}) of DEA NONOate at 25 °C and pH 7.0 is approximately 0.0007 s^{-1} [46]. The conditions used in our NO and O_2 competition studies. The DEA NONOate decomposition is characterized by first-order release kinetics [47], and thus, for the NO donor (N), we can write:

$$[N] = [N]_0 e^{(-k_{dec} t)} \quad (1)$$

Using this formula, the concentration of DEA NONOate as a function of time is obtained for an initial NO concentration of 16 μM (used in NO and O_2 competition studies). Each mole of DEA NONOate releases circa 1.5 moles of NO [47]. Hence, the amount of NO released for an initial DEA NONOate concentration of 16 μM is predicted. This amount is much less than 1 μM·s^{-1} at any time point. The NO release rate is defined by the mass conservation equation [47]:

$$\frac{d[NO]}{dt} = \text{NO release rate} - 4k^*[NO]^2[O_2] - (k_L a/V)[NO] \quad (2)$$

The second term is the molar rate at which NO reacts with O_2, and the third term is the molar rate at which NO leaves the solution. Since no stirring was used during the NO reaction in our experiment, the last term is negligible. On the other hand, for the second term describing the NO reaction with O_2 in air with normal composition, the O_2 partial pressure is 0.21 atm. Thus, the O_2 solubility is 254 μM in normal pure water [48]. For a well-stirred experimental setup at 37 °C, the k^* is 2.4×10^6 ($M^{-2}S^{-1}$). Using

this k^* value (which is an overestimated), the amount of NO reacted with O_2 at any time is negligible. Therefore, in our setup with no stirring and at 25 °C, the reaction between NO and O_2 is insignificant (see Results). Consequently, the amount of NO in the solution is approximately equal to the amount of NO generated by the decomposition of DEA NONOate.

NO trap experiments

A stock solution (21 μM) of *N*,*N*,*N*′,*N*′-tetramethyl-p-phenylenediamine (Sigma Aldrich, St. Louis, MO, USA), the NO-trap reagent, was prepared under anaerobic conditions by dissolving the compound in the anaerobic phosphate buffer (pH 7.0). The vial was immediately covered with aluminium foil to protect it from light exposure. Separately, a stock solution of DEA NONOate was prepared in phosphate buffer (pH 7.0) under aerobic conditions at the same concentration as the NO trap solution. Immediately, 50 μL of the DEA NONOate stock solution was diluted into 600 μL of phosphate buffer in a plastic cuvette. A total of five samples were prepared, and one control cuvette contained only phosphate buffer. All samples and the control were incubated under aerobic conditions. At time 0 (t), 50 μL of the NO trap solution was added to the control cuvette and one sample cuvette. Each cuvette was gently shaken to ensure thorough mixing, and the UV–visible absorbance was measured immediately. Subsequent measurements were conducted hourly after incubating samples aerobically: every 60 min, 50 μL of the NO trap solution was added to one additional sample cuvette, mixed by gentle shaking and the UV–visible absorbance spectrum was recorded.

Exposure to pioglitazone and gasotransmitters

Pioglitazone was added before or after exposure to NO under anaerobic conditions at room temperature (22 °C). First, 50 μL purified protein solution was added to phosphate buffer pH 7.0 (calculated for a total reaction volume of 700 μL), followed by the addition of 50-μL pioglitazone solution. The sample was incubated for 2 h, and then 50 μL NO-donor solution was added to the protein and mixed thoroughly. The sample was then incubated overnight under anaerobic conditions (22 °C) to ensure complete removal of unreacted NO. The next day, 50 μL of H_2S donor was added, and the mixture was incubated for 4 h. In another sample, pioglitazone was added after the addition of DEA NONOate. To this end, after adding DEA NONOate, the sample was incubated in the glovebox under anaerobic conditions (22 °C) overnight for NO exposure and removing any residual NO. The next day, 50-μL pioglitazone solution was added under anaerobic conditions (22 °C), and the mixture was for 2 h at room temperature under anaerobic conditions. Finally, 50 μL H_2S-donor solution was added to the mixture, and the sample was incubated for 4 h in the anaerobic glovebox. UV–visible absorbance spectrum was recorded at each step before and after adding pioglitazone, NO and H_2S. The NO donor-, H_2S donor- and pioglitazone-to-mitoNEET ratio was 1.

UV–visible spectrophotometry

To record the UV–visible absorbance spectra, samples were added anaerobically to a 1-mL disposable plastic cuvette (BRAND™, Willimantic, CT, USA) with a path length of 1 cm and equipped with a silicone lid (BRAND™) to tightly close and prevent oxygen exposure. Each sample was transported outside, and the UV–visible absorbance spectrum was recorded immediately. Measurements were done at room temperature using a PerkinElmer UV/Vis Lambda 365 Instrument (Shelton, CT, USA). Spectra were recorded from 300 to 700 nm, which is the wavelength window used by others to study mitoNEET [32,38]. Measurements were done at room temperature (22 °C) under aerobic conditions.

Preparation of samples for liquid chromatography–mass spectrometry analysis (LC–MS) of 3 -deoxy-3 ,4 -didehydro-CTP (ddhCTP) formation

Anaerobic buffer, 50 mM MOPS, pH 7.0, containing 100 mM NaCl, was used to prepare stock solutions of SAM, cytidine triphosphate (CTP), H_2S donor and sodium dithionite under anaerobic conditions in a glovebox (Belle Technology ($O_2 < 5$ ppm)). An aliquot of chemicals was transported into the glovebox and mixed with the buffer under anaerobic conditions. The buffer was prepared a day prior to the experiments and stored in the glovebox overnight to ensure complete anaerobicity. Four samples were prepared. The complete reaction had 500 μL of purified hSAND solution, 20 μL SAM chloride (S-(5′-adenosyl)-L-methionine-(S-methyl-13C) chloride), 20 μL CTP (cytidine 5′-triphosphate disodium salt) and 20 μL $Na_2S_2O_4$ (sodium dithionite). The anaerobic MOPS buffer pH 7.0 was added to reach a final volume of 660 μL. A negative control sample was prepared. In the negative control, hSAND was not added, and it was replaced with buffer and NADH. The reaction mixture was incubated anaerobically overnight. The following day, the sample was centrifuged at 16250 x g for 3 min. Then, 450 μL of the reaction was added to a 0.5-mL Amicon Ultra Centrifugal Filters 3 kDa (Merck) and centrifuged at 16250 x g for 30 min. The resulting flow-through was then carefully transferred to an HPLC low volume (300 μl) recovery vial (Fisher Scientific) and sealed tightly with a polypropylene cap (Fisher Scientific). Each experiment was repeated at least two times with different batches of protein to test reproducibility.

To test the activity of hSAND exposed to H_2S, we prepared three samples. Sample 1, hSAND exposed to H_2S

only: 200 µL of 140 µM purified hSAND solution was mixed with 10 µL of stock solution of H_2S donor, then the mixture was incubated under anaerobic condition for 2 h, followed by the added 10 µL SAM, 10 µL CTP and 10 µL of anaerobic MOPS buffer pH 7.0 to reach a final volume of 250 µL. Sample 2, hSAND exposed to H_2S and $(S_2O_4)^{2-}$: 200 µL of 140 µM purified hSAND solution was exposed to 10 µL stock solution of H_2S donor for 2 h. Next, 10 µL of sodium dithionite was added, followed by the addition of 10 µL of SAM and 10 µL of CTP. Sample 3, the control hSAND sample not exposed to H_2S: 200 µL of 140 µM purified hSAND solution was mixed with 10 µL of sodium dithionite, 10 µL of SAM and 10 µL of CTP and 10 µL of buffer anaerobic MOPS, buffer pH 7.0 to reach a final volume of 250 µL. Samples were incubated overnight, subject to filtration using 3 kDa Amicon ultracentrifugal filter to remove proteins and the flowthrough was used to measure the formation of ddhCTP from CTP. Experiments were repeated at least two times to confirm reproducibility.

LC–MS

Measurements were performed using an Agilent InfinityLab G6160A LC/MSD iQ mass spectrometer equipped with [Agilent 1260 Infinity II] liquid chromatography system. Coumn was Agilent ZORBAX RR HILIC Plus Column, 2.1 x 100 mm, 3.5 µm. Instrument control and data processing were performed using OPENLAB CDS (Agilent Technologies, Santa Clara, CA, USA). The system was calibrated on the day of the analysis. Electrospray source conditions were adjusted to maximize sensitivity, and the detection mode was set to detect negative (−) ions. For each run, 50 µL of solution was injected with a flow rate of 0.2 mL·min^{-1} and an oven temperature of 45 °C:

- Buffer A: 90 vol.% MeCN (acetonitrile) (Fisher, 99.9%): 10 vol.% LC–MS grade water (Fisher), 20 mM ammonium acetate, pH 7.4–7.5.
- Buffer B: 10 vol.% LC–MS grade water (Fisher), 20 mM ammonium acetate, pH 7.4–7.5.
- Column:
- Flow rate: 0.2 mL·min^{-1}
- Gradient: [0–1 min]: 100 : 0 (A : B); [1–10 min] 100 : 0 (A : B) linearly changed to 10 : 90 (A : B); [10–15 min] 10 : 90 (A : B); [15 : 17] linearly changed to 100 : 0 (A : B) and [17–35 min] 100–0 (A : B).

Analysis of the LC–MS data was performed using OPENLAB CDS software.

Preparation of sample for electron paramagnetic resonance (EPR) spectroscopy

Anaerobic buffer (50 mM phosphate, pH 7.0, 100 mM NaCl) was used to prepare different reagents used in experiments. All reagents were transported into the glovebox and mixed with the buffer under anaerobic conditions. The buffer was prepared a day prior to the experiments and stored in the glovebox overnight to ensure complete removal of dioxygen. For NO and H_2S exposed, the NO or H_2S donor was dissolved in buffer and immediately added to the solutions. To prepare the samples, components were added in the following order: 150 µL purified protein solution, phosphate buffer (an aliquot added to make up a total volume of 200 µL), 20 µL $(S_2O_4)^{2-}$ (for reduced samples only) and 20 µL reagent solution. The molecular ratio of NO donor, H_2S donor or $(S_2O_4)^{2-}$ to protein was 1. Samples were incubated overnight under anaerobic conditions. Next, they were transferred into 3 mm ID, 4 mm OD or 1.1 mm ID, and 1.6 mm OD clear fused quartz EPR tubes (Wilmad 707-SQ-250M and Wilmad WG-221T-RB, respectively). Samples were transferred to the outside of the glovebox and frozen immediately in liquid nitrogen.

Additional methods

Details of EPR measurements and molecular dynamics (MD) simulations are available in Data S1.

Results

NO degrades hSAND cluster

The reaction of O_2, H_2O_2 and NO with most [Fe-S] proteins leads to the degradation of the cluster. To have a system for comparing the degradation reaction with the sensory reaction, we first investigated the reaction of O_2, H_2O_2 and NO with the hSAND [4Fe-4S] cluster, which has not been studied. We first overexpressed and purified the hSAND soluble form lacking the N-terminus hydrophobic membrane anchoring domain. Next, we used a combination of spectroscopic methods and LC–MS and investigated the effect of gasotransmitter NO on the hSAND [4Fe-4S] cluster. We compared the results with those we obtained from the effect of other oxidizing agents, namely, dissolved O_2 gas and H_2O_2. The purified hSAND was in the oxidized state (Fig. 2A), and the addition of sodium dithionite reduced the cluster as observed by the disappearance of the UV–visible absorbance peak of the $[4Fe\text{-}4S]^{2+}$ cluster between 400 and 450 nm (Fig. 2A). The enzyme with the reduced cluster was active and capable of converting CTP to its nucleotide analogue ddhCTP [49,50], as measured by LC–MS (Fig. 2B). Exposure of oxidized $[4Fe\text{-}4S]^{2+}$ cluster to O_2 (Fig. S1A) or H_2O_2 (Fig. S1B) led to the disappearance of the absorbance peak of the $[4Fe\text{-}4S]^{2+}$ cluster, suggesting degradation of the cluster consistent with our previous observation of O_2-mediated degradation of the fungal SAND cluster [51]. Similarly, the NO

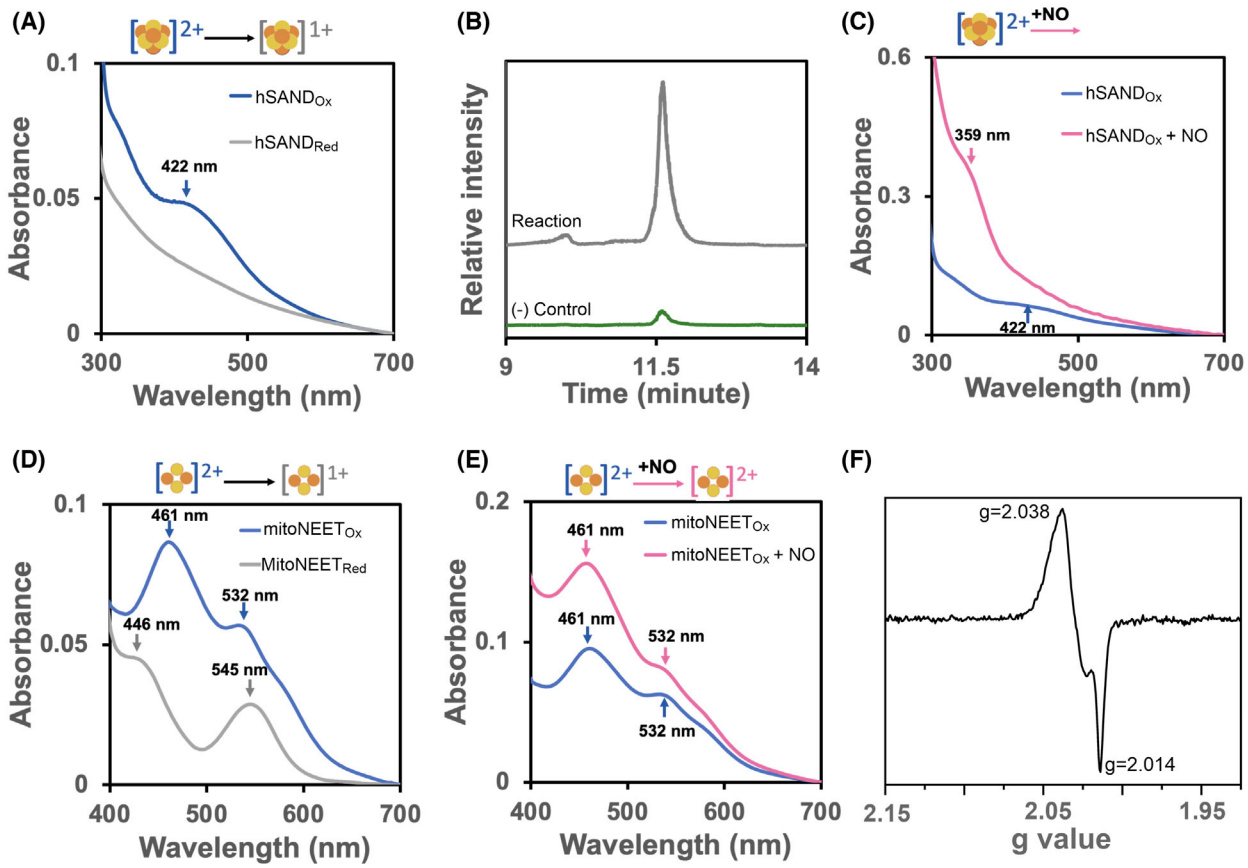

Fig. 2. The SAND [4Fe-4S] cluster and mitoNEET [2Fe-2S] cluster react with NO differently. (A) UV–visible absorbance spectrum of hSAND (5 ± 1 μM) [4Fe-4S] cluster before (hSAND$_{Ox}$) (blue) or after (hSAND$_{Red}$) (grey) reduction (30 min) by sodium dithionite ($(S_2O_4)^{2-}$) (5 μM). (B) LC–MS analysis of the formation of ddhCTP. The graph shows the extracted ion chromatograph (EIC) of ddhCTP with a $[M\text{-}H]^{-1}$ m/z of 464.0. The reaction contained hSAND (53 μM), $(S_2O_4)^{2-}$ (5.3 mM), SAM (21.2 mM) and CTP (5.3 mM). The negative control did not have hSAND. (C) The reaction of oxidized hSAND [4Fe-4S] cluster (8 μM) with NO released (4 h) from DEA NONOate (8 mM). (D) The UV–visible absorbance spectrum of mitoNEET [2Fe-2S] cluster (10 ± 2.65 μM) before (mitoNEET$_{Ox}$) (blue) and after (mitoNEET$_{Red}$) (grey) reduction (30 min) by sodium dithionite ($(S_2O_4)^{2-}$) (10 μM). (E) The reaction of oxidized mitoNEET $[2Fe\text{-}2S]^{2+}$ cluster (10 μM) with NO released (4 h) from NONOate (1 mM). (F) CW-EPR spectrum at T = 40 K of mitoNEET $[2Fe\text{-}2S]^{2+}$ cluster (200 μM) oxidized with NO released from DEA NONOate (215 μM), incubated overnight under anaerobic conditions. (A–E) Were repeated three times, and (F) was repeated two times to confirm reproducibility. Buffers were (A, C–F) phosphate 50 mM, 100 mM NaCl, pH 7.0 and (B) MOPS 50 mM, 100 mM NaCl, pH 7.0. All samples were prepared at room temperature (~ 22 °C) under anaerobic conditions ($O_2 < 5$ ppm).

released by the NO-donor agent dimethylamine NONOate (DEA NONOate) under anaerobic conditions degrades the hSAND cluster. The exposure of the oxidized (Fig. 2C) or reduced (Fig. S1C) hSAND to NO led to the disappearance of the $[4Fe\text{-}4S]^{2+}$ cluster absorbance peak at 400–450 nm and the appearance of a new peak with a maximum absorbance of approximately 359 nm. The observation of this peak is somewhat similar to that reported previously for iron-nitrosyl complexes [52]. While NO-exposed enzyme completely lost its ability to catalyse the transformation of CTP to ddhCTP, the O_2- and H_2O_2-exposed enzymes retained approximately 30% and 10% of their activities, respectively (Fig. S1D). These data confirmed that NO, O_2 and H_2O_2 degrade the hSAND cluster and that NO degradation is more severe. Therefore, NO reacts with the [4Fe-4S] cluster and degrades it, generating iron-nitrosyl species, possibly like those observed by NO-mediated degradation of [4Fe-4S] cluster of NO sensory proteins [53].

mitoNEET [2Fe-2S] cluster senses NO in a specific way

Next, we purified a soluble form of mitoNEET lacking the N-terminus hydrophobic domain and studied how

NO, O_2 or H_2O_2 react with its cluster. The individual reaction of O_2, H_2O_2 or NO with mitoNEET [2Fe-2S] cluster has been studied extensively previously [31–40]. We repeated these experiments to understand the system and be able to further investigate the molecular mechanism of the reaction of NO and the interplay among NO, O_2 and H_2S reactions with the mitoNEET [2Fe-2S] cluster, unlike previous works [31–40]. The purified mitoNEET showed two absorbance peaks at 461 and 532 nm, typical of the oxidized $[2Fe\text{-}2S]^{2+}$ clusters and the cluster was reduced by sodium dithionite showing two absorbance peaks at 446 and 545 nm (Fig. 2D). For subsequent studies with mitoNEET, we chose the more physiologically relevant phosphate buffer (pH 7.0) since, unlike MOPS buffer, it did not affect the mitoNEET-oxidized cluster (Fig. S2A). Unlike hSAND, whose cluster was degraded by NO, O_2 or H_2O_2, the mitoNEET [2Fe-2S] cluster was not and reacted differently with each molecule. The exposure of oxidized mitoNEET $[2Fe\text{-}2S]^{2+}$ cluster to H_2O_2 or O_2 did not affect the cluster (Fig. S2B,C). Both O_2 and H_2O_2 were able to oxidize the reduced $[2Fe\text{-}2S]^{1+}$ cluster (Fig. S2D,E). Exposure of the oxidized (Fig. 2E) or reduced (Fig. S2F) cluster to NO released from NO donor generated an oxidized form of $[2Fe\text{-}2S]^{2+}$ cluster with a higher absorbance than that of the as-isolated oxidized protein. The addition of sodium dithionite reduced the NO-exposed cluster, generating an absorbance spectrum identical to that of the reduced cluster not exposed to NO (Fig. S2G). Therefore, NO oxidizes the [2Fe-2S] cluster but does not degrade it unlike what we observed for hSAND. The ability of the mitoNEET cluster (midpoint redox potential of +35 mV) to be oxidized by NO is consistent with the most cited standard potential value of +390 mV (1 M vs. NHE) for the $NO/^3NO^-$ couple [54]. The increase in the absorbance of the NO-exposed cluster (Fig. 2E), as compared to the O_2-oxidized cluster (Fig. S2D), may suggest possible coordination of NO to the cluster as reported by others for the NEET family of proteins [38–40,55]. To test this possibility, we exposed the oxidized $[2Fe\text{-}2S]^{2+}$ cluster to NO and performed continuous-wave (CW) X-band EPR spectroscopy measurements (Fig. S2H). To prevent any background signal from NO, samples were prepared by incubating mitoNEET and NO donor (the DEA NONOate) in a one-to-one ratio and overnight incubation in the glovebox (Data S1) to allow removal of any excess NO. EPR measurements (Fig. 2F) revealed the presence of a signal identical to that reported for iron-nitrosyls coordinated with cysteine residues of a protein [56,57]. The percentage of iron-nitrosyl species, as determined by comparison of the relative CW-EPR signal intensities, was a fraction ($\sim 5\%$) of the total reduced cluster. When we exposed the oxidize $[2Fe\text{-}2S]^{2+}$ cluster to different DEA NONOate-to-protein ratios, at the ratio above 50, we observed a significant increase in the UV–visible absorbance spectrum of the cluster (Fig. S2I). Therefore, mitoNEET [2Fe-2S] cluster reacts with NO in a specific way.

Discovery of an NO access site to mitoNEET [2Fe-2S] cluster

It is unknown how NO reaches the mitoNEET cluster, and previous works have not explored this mechanism [31–40]. To gain insight into this mechanism, we first used MD simulations to study the interaction of NO and H_2O_2 with mitoNEET (Data S1). The average backbone RMSD (root-mean-square deviation) values of the protein for 50 ns were less than 2 Å (Fig. S3A), indicating that the system is in a thermal equilibrium. Next, we compared the root-mean-square fluctuation (RMSF) of C-α atoms to assess the protein flexibility in the presence of H_2O_2 or NO (Fig. S3B). Protein flexibility in the presence of H_2O_2 or NO is similar, with average RMSF values being 0.62 ± 0.37 or 0.6 ± 0.34, respectively. Analysis of the interaction between NO or H_2O_2 molecules with the mitoNEET residues located in the vicinity of the [2Fe-2S] cluster (Fig. 3A and Table S1) showed that H_2O_2 largely forms stable hydrogen bonds with the side chains of residues on the protein surface such as Arg76, Lys78, Lys79 and Asp84; while NO forms hydrogen bonds with residues at the interface of the dimer, namely, Tyr71 and Arg73 (Fig. 3B). Thus, while NO diffuses into the protein shell, H_2O_2 cannot. Using the CAVER WEB 1.0 server, we identified 19 possible (Fig. S3C) NO access tunnels. Most of these tunnels are formed at the interface between two mitoNEET monomers, but tunnel 1 entry site is located directly on the surface at the top of the cluster (Fig. 3C). This short tunnel is notable because it enables direct access to the cluster (Fig. 3C). A total of 19 amino acid residues are involved in the construction of tunnel 1 (Table S2). Four key residues of the entry site of the tunnel, namely, Val70, Pro100, Leu101 and Ile102, cannot participate in hydrogen bonding with NO, thus allowing it accessibility to the [2Fe-2S] cluster. Consistently, the NO trajectory in the MD simulations shows direct movement towards the cluster through this entry site (Fig. S4A), while for H_2O_2, there is no direct path due to the multiple hydrogen bonds it forms with surface residues (Fig. S4B). Additionally, the results of MD calculations predict that NO remains near the cluster for a significantly longer period than H_2O_2. The

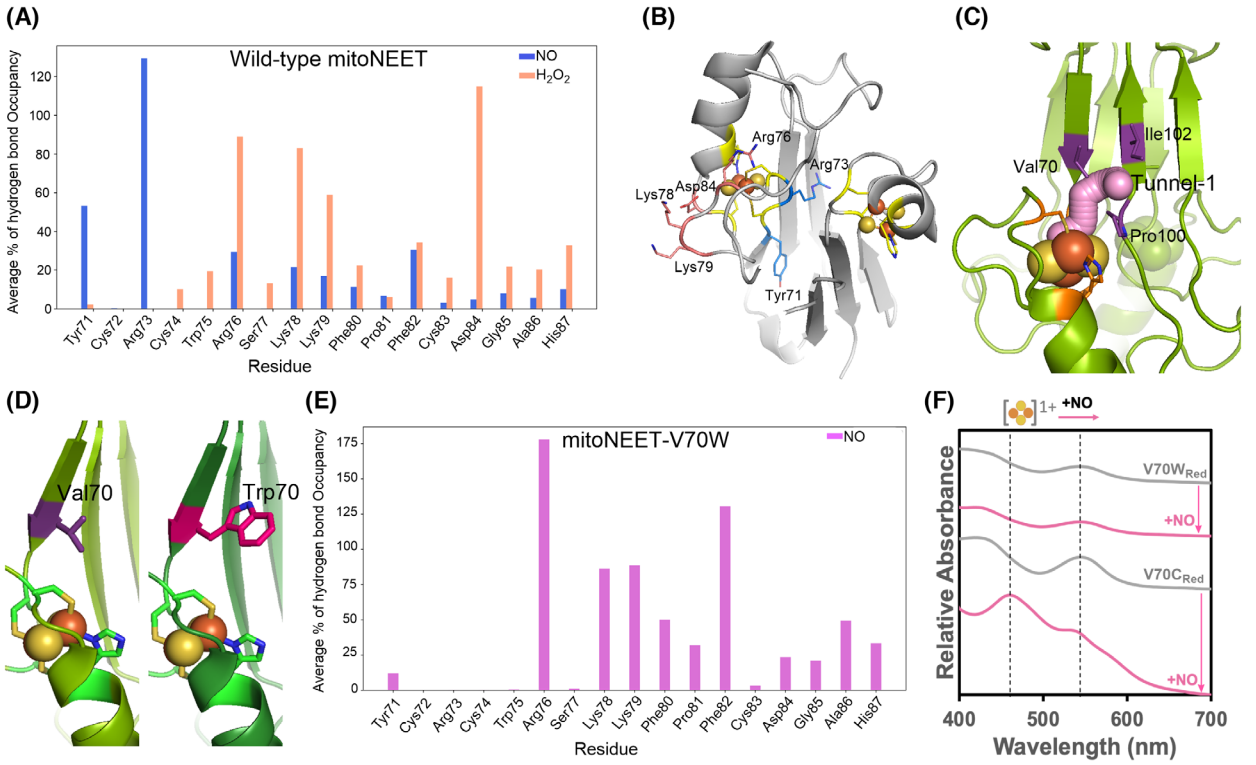

Fig. 3. NO reaches the mitoNEET [2Fe-2S] cluster through an explicit access site. (A) The average % of hydrogen bond occupancy with the residues within 3.5 Å of the [2Fe-2S] cluster. (B) The structure (PDB code 2QH7) shows residues at the dimer interface interacting with NO (blue) and the main surface residues interacting with H_2O_2 (salmon). (C) Schematic presentation of the predicted tunnel 1 with the shortest distance to the cluster. (D) A comparison of the WT and V70W mitoNEET structures suggests that tryptophane covers, at least partially, NO access to the cluster through tunnel 1. (E) The average % of hydrogen bonds formed between NO molecule and individual residues of the mitoNEET-V70W variant during the last 50 ns of the NO-diffusion simulation repeats. (A, E) Hydrogen bonds were identified by using the cut-off distance of 3.5 Å between hydrogen bond donor/acceptor atoms and a bond angle cut-off of 120°. (F) NO cannot oxidize the reduced $[2Fe\text{-}2S]^{1+}$ cluster of the V70W variant (14 μM), but it oxidizes that of the V70C variant (25 μM). Oxidized mitoNEET was reduced with an equivalent amount of dithionite ($(S_2O_4)^{2-}$) and then subject to NO reaction. Proteins were incubated with the NO-donor agent for 4 h under anaerobic conditions at room temperature (~ 22 °C). The difference between V70W and V70C variants confirms that all dithionite is consumed and does not affect NO oxidation. The ratio of the NO-donor concentration to that of mitoNEET was 1. Buffer was phosphate 50 mM, 100 mM NaCl, pH 7.

survival probability, defined as the fraction of ligands that remain intact over time, of H_2O_2 drops to 0% within just 5 ns, while NO maintains a survival probability of 86% even after 20 ns (Fig. S4C). These findings suggest a specific NO entry site to the mitoNEET [2Fe-2S] cluster. To validate the result of the predictions, we created two variants. We replaced the highly conserved Val70 of the entry site with the bulky residue tryptophane (mitoNEET-V70W), hypothesizing that this mutation will cap the NO entry site, abolishing NO access to the cluster. In the second variant, Val70 was replaced with a cysteine (mitoNEET-V70C) to further facilitate NO access and reaction. The predicted structure of V70W variant shows that tryptophane covers the entry site, possibly blocking NO access (Fig. 3D), while in the V70C variant, the entry site was accessible (Fig. S4D). Analysis of the interaction of NO with mitoNEET-V70W (Fig. 3E) and -V70C (Fig. S4E) residues located in the vicinity of the [2Fe-2S] cluster revealed that V70W mutation completely abolished the NO interaction with Tyr71 and Arg73 at the interface of two mitoNEET subunits (Fig. 3E), while V70C mutation slightly increased the interactions as compared to wild-type protein (Fig. S4E). This analysis suggests that in the V70W variant, NO cannot diffuse into the protein. Next, both variants of mitoNEET were purified and characterized. The reduced and oxidized variants have a UV–visible absorbance spectrum the same as the reduced and oxidized wild-type (WT) proteins, respectively (Fig. S5A,B). Additionally, EPR spectroscopy confirmed that both clusters were reduced the same as the

wild-type mitoNEET [2Fe-2S] cluster (Fig. S5C,D). Therefore, neither mutation affected the [2Fe-2S] cluster. Subsequently, we studied the reaction of NO with the reduced or oxidized clusters. NO was unable to oxidize the reduced $[2Fe\text{-}2S]^{1+}$ cluster of the V70W variant (Fig. 3F), unlike what we observed for wild-type mitoNEET. In contrast, NO was able to reduce the $[2Fe\text{-}2S]^{1+}$ cluster of the V70C variant (Fig. 3F). Additionally, exposure of the oxidized mitoNEET-V70W variant to NO did not increase the absorbance (Fig. S5E), but that of oxidized mitoNEET-V70C variant did (Fig. S5F), similar to what we observed for wild-type protein (Fig. 2E). These findings confirm that the V70W mutation blocked NO access to the cluster. In summary, MD simulations and mutagenesis studies confirm that NO diffuses towards the mitoNEET [2Fe-2S] cluster through an explicit NO tunnel with an entry site on the surface near the cluster.

Gasotransmitter H_2S reduces mitoNEET [2Fe-2S] cluster

While the reaction of biological thiols such as reduced glutathione (GSH) or cysteine with mitoNEET has been studied [35], the reaction of gasotransmitter H_2S with mitoNEET cluster and other [Fe-S] proteins is unknown. Therefore, we tested how H_2S can affect hSAND and mitoNEET redox state. We first tested the reduction of hSAND [4Fe-4S] cluster by H_2S. The redox potential of the [4Fe-4S] cluster in some radical-SAM enzymes is predicted to fall in the range of −500 and −450 mV [16], and the two-electron redox potential of H_2S is +0.17 mV at pH 7.0 [58]. These redox potentials suggest that H_2S is unlikely to reduce the [4Fe-4S] cluster of hSAND. Consistently, we observed that H_2S did not reduce the hSAND cluster. When the oxidized hSAND was exposed to H_2S, the absorbance peak of the $[4Fe\text{-}4S]^{2+}$ cluster changed (Fig. 4A). However, this change was not observed when the reduced protein was exposed to H_2S (Fig. S6A). The CW EPR measurement showed that H_2S did not reduce the $[4Fe\text{-}4S]^{2+}$ cluster (Fig. S6B). This observation was further confirmed by LC–MS analysis of ddhCTP formation showing that the H_2S-exposed enzyme was unable to catalyse transformation of CTP to ddhCTP (Fig. 4B).

On the other hand, the midpoint redox potential of mitoNEET is measured to be +35 mV (at pH 7.5) [59], suggesting that it can be reduced by H_2S. Consistently, we found that exposure of the oxidized mitoNEET cluster to H_2S donor generated the reduced $[2Fe\text{-}2S]^{1+}$ cluster with absorbance peaks at 446 and 545 nm (Fig. 4C). When mitoNEET was first reduced by sodium dithionite ($(S_2O_4)^{2-}$), it was not further reduced by the addition of H_2S. The UV–visible absorbance spectra of mitoNEET reduced by H_2S released from H_2S donor or sodium dithionite were similar (Fig. S6C). EPR spectroscopy confirmed that the H_2S- and dithionite-reduced $[2Fe\text{-}2S]^{1+}$ clusters are structurally similar. The CW measurements showed that both samples were reduced (Fig. S6D). Both spectra showed characteristic features of the dipolar interaction between the electron spins of the two adjacent reduced clusters in the dimeric unit of mitoNEET, as described previously [60,61]. These features were less prominent in the spectrum of the H_2S-reduced sample compared to the one reduced by dithionite, consistent with a lower spin count (~70%). Hyperfine sublevel correlation (HYSCORE) measurements confirmed that the environment of the [2Fe-2S] cluster was unchanged. The major peaks in the HYSCORE spectra correspond to those previously assigned to the $[2Fe\text{-}2S](Cys)_3(His)$ cluster in rat mitoNEET, including those arising from the nitrogen ligand of the histidine and are the same for dithionite and H_2S reduced cluster (Fig. 4D) [61]. To get further insights into the potential diffusion of H_2S into the mitoNEET structure, we performed MD simulations. Like NO, the backbone RMSD values of around 2 Å relative to the initial crystal geometry (Fig. S6E) indicate thermal structural stability and minimal conformational changes in the system. The RMSF of C-α atoms in the presence of H_2S (Fig. S6F) revealed that the protein flexibility is like that in the presence of NO. Similar to NO and unlike H_2O_2, the highest hydrogen bond occupancy was observed with the side chain of Arg73 located in the interface between the dimers (Fig. S6G). Additionally, the survival probability of H_2S remains around 90% after 20 ns (Fig. 4E) suggesting stronger interaction of H_2S as compared to NO, whose survival probability was 86%. We observed that H_2S reduced the oxidized cluster of the V70W and V70C variants of mitoNEET (Fig. S6H,I). This observation suggests that H_2S either reaches the cluster through other predicted tunnels or does not need to react directly with the cluster to reduce it.

Pioglitazone blocks NO access

It is unknown if the reaction of NO with the mitoNEET [2Fe-2S] cluster affects its ability to be reduced by biologically relevant reducing agents such as H_2S. To address this question, we tested if H_2S can reduce the mitoNEET $[2Fe\text{-}2S]^{2+}$ cluster after its exposure to O_2 or NO, the latter in the presence of very low O_2 level (circa 5 ppm) (approximately 7 nM). We found

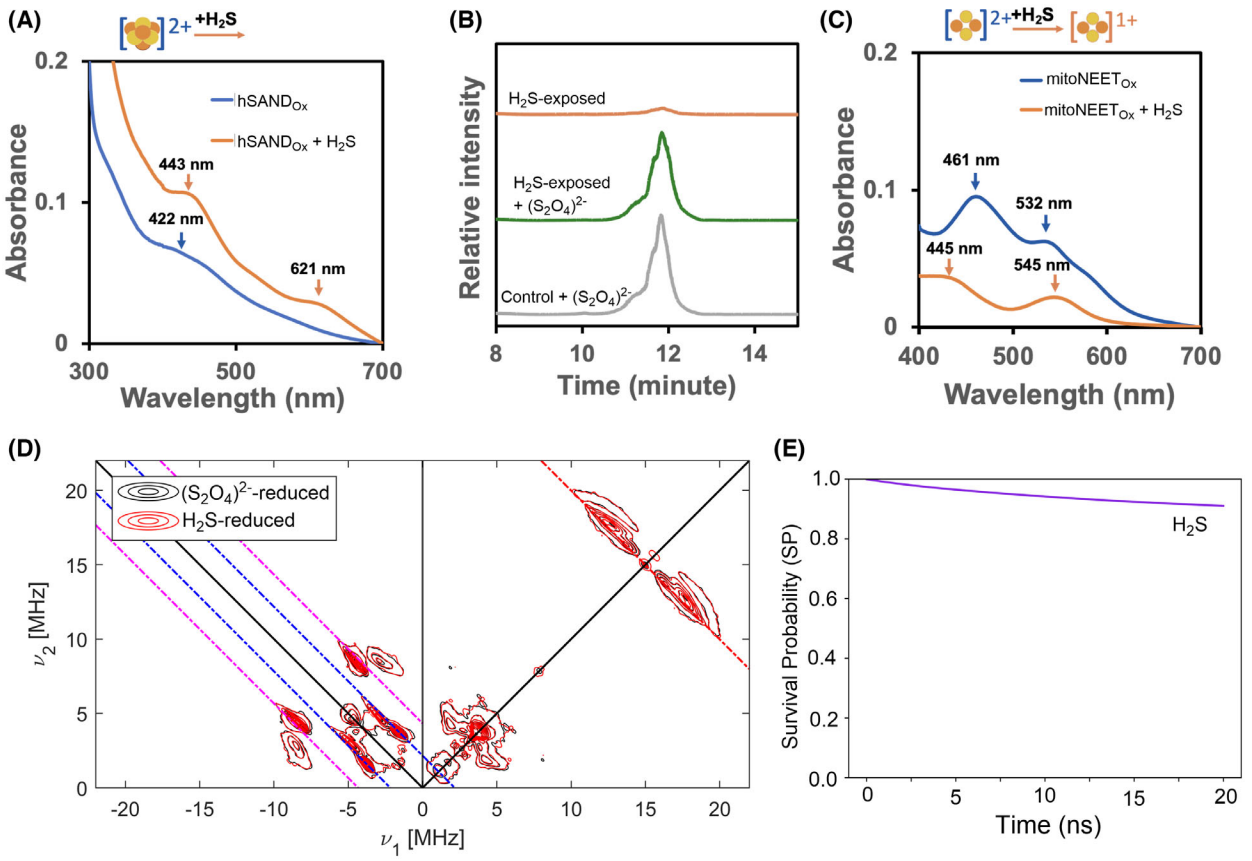

Fig. 4. Gasotransmitter H_2S reduces the mitoNEET [2Fe-2S] cluster. (A) The reaction of oxidized hSAND (8 μM) with H_2S (H_2S donor 3.6 mM) (4 h). (B) The hSAND [4Fe-4S] cluster is catalytically active after exposure to H_2S (4 h). The graph shows the extracted ion chromatogram of ddhCTP ($[M\text{-}H]^{-1}$ m/z of 464.0) generated by hSAND exposed to H_2S only (orange), to H_2S and then reduced by dithionite ($(S_2O_4)^{2-}$) (green) or reduced by $(S_2O_4)^{2-}$ only (grey). The SAM, CTP and $(S_2O_4)^{2-}$ concentrations were 44.8, 11.2 and 11.2 mM, respectively, and those of hSAND and H_2S donor were 112 μM. (C) H_2S reduces the oxidized mitoNEET $[2Fe\text{-}2S]^{2+}$ cluster. mitoNEET (10 μM) was incubated with H_2S donor (10 M) for 4 h, and the spectra were recorded before and after. (D) HYSCORE spectra at 10 K of dithionite-reduced (black contour lines) and H_2S-reduced (red contour lines) mitoNEET [2Fe-2S] cluster. The red, blue and magenta dashed lines designate the ^1H, ^{14}N single-quantum and ^{14}N double-quantum frequencies respectively. The concentrations of mitoNEET, H_2S donor and $(S_2O_4)^{2-}$ were 200, 430 and 215 μM respectively. (E) The survival probability of H_2S interaction with mitoNEET. (A–C) All experiments were repeated three times, and (D) the experiment was repeated two times to confirm reproducibility. Buffer was (A, C) phosphate 50 mM, 100 mM NaCl, pH 7.0 or (B) MOPS 50 mM, 100 mM NaCl, pH 7.0. (A–D) Samples were prepared at room temperature (~ 22 °C) under anaerobic conditions.

that H_2S reduced the O_2-oxidized cluster (Fig. S7A) like sodium dithionite (Fig. S7B), but it did not reduce the NO-exposed cluster when the O_2 level was low (Fig. 5A), unlike sodium dithionite (Fig. S2G). The ability of H_2S to reduce the cluster was dependent on the amount of NO used. At a NO-to-mitoNEET ratio of 0.5, only about half the clusters could be reduced as the absorbance of the oxidized cluster decreased circa 50% (Fig. S7C). At a NO-to-mitoNEET ratio of 1 or more, H_2S could not reduce any of the clusters, and the absorbance of the NO-exposed oxidized cluster did not change after exposure to H_2S (Fig. S7C). Conversely, NO was able to oxidize the H_2S-reduced cluster (Fig. S7D). These findings confirm that when the O_2 level is low, the reaction of NO with mitoNEET [2Fe-2S] cluster desensitizes it towards reduction by gasotransmitter H_2S. It is known that type 2 diabetic drug pioglitazone interacts with mitoNEET and attenuates mitochondrial oxidative damage [62,63]. However, the exact mechanism of pioglitazone action is unknown. We hypothesized that TZD ligands like pioglitazone may protect mitoNEET against oxidation by NO and, therefore prevent desensitization towards H_2S reduction. Previous structural studies revealed that TZD ligands like sulphonamide (Fig. S7E) bind on the surface of the mitoNEET cluster, interacting with amino acid residues we predicted to form the entry site of tunnel 1. Similarly, our docking studies

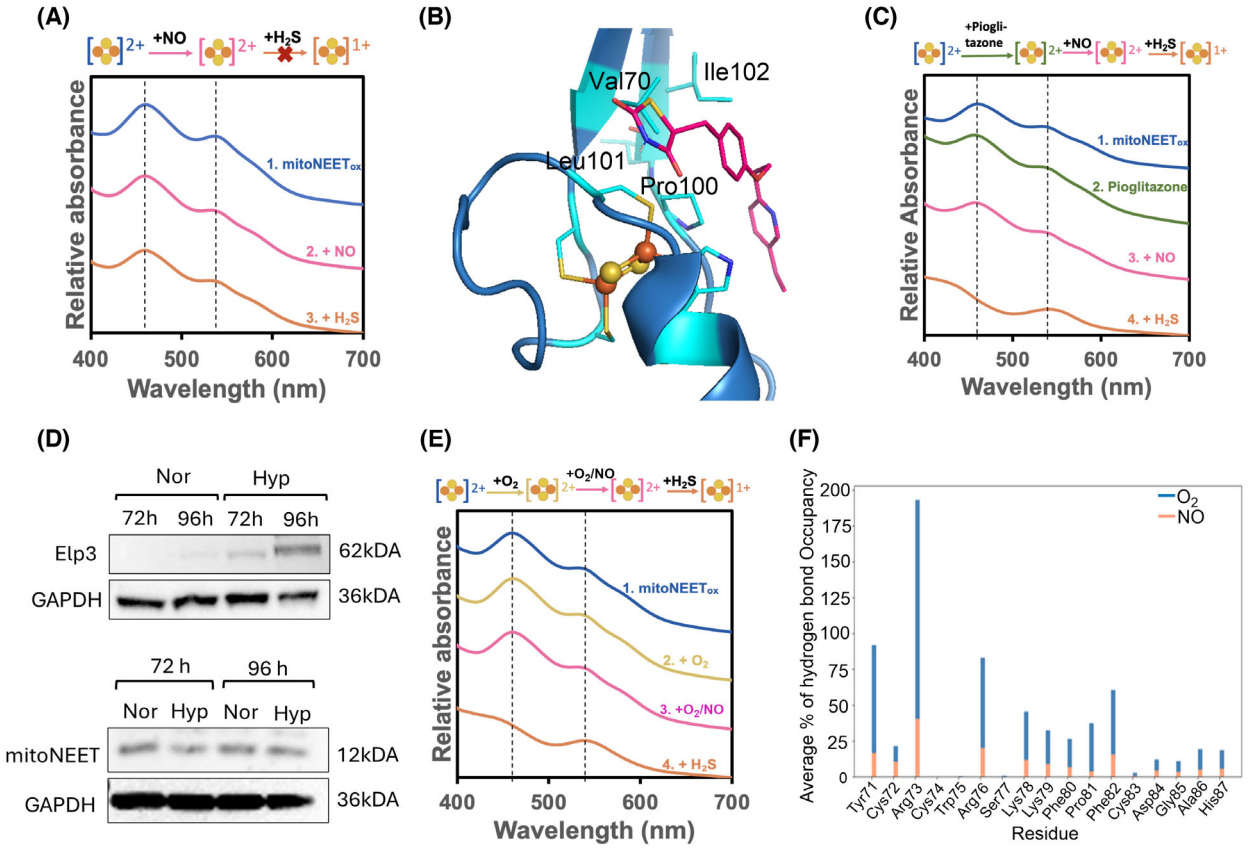

Fig. 5. O_2 and pioglitazone block the NO access to the mitoNEET $[2Fe\text{-}2S]^{2+}$ cluster. (A) Exposure of the anaerobically NO-exposed (overnight) oxidized mitoNEET $[2Fe\text{-}2S]^{2+}$ cluster to H_2S released from H_2S donor (4 h under anaerobic conditions) does not reduce the cluster. (B) Docking of pioglitazone using the structure of mitoNEET (PDB Code: 3REE) predicts its binding to the residues forming the NO entry site, residues Val70, Pro100, Leu101 and Ile102. (C) The addition of pioglitazone before NO exposure (overnight under anaerobic conditions) restores the ability of H_2S released from H_2S donor (4 h under anaerobic conditions) to reduce the NO-exposed mitoNEET $[2Fe\text{-}2S]^{2+}$ cluster. (D) Western blot analysis of the expression of Elp3 (62 kDa) ($[4Fe\text{-}4S](Cys)_3$ cluster) and mitoNEET (15 kDa) in T_{effs} under hypoxic (Hyp) or normoxic (Nor) conditions. GAPDH was used as a loading control. (E) H_2S reduces aerobically NO-exposed (O_2/NO-exposed cluster) mitoNEET. The mitoNEET cluster was exposed to NO (4 h) under aerobic conditions (O_2/NO-exposed cluster) and subsequently incubated under anaerobic conditions (overnight) and then exposed to H_2S (4 h under anaerobic conditions). (F) The average % of hydrogen bond occupancy with the residues near the [2Fe-2S] cluster. The graph shows O_2 occupancy in the presence of NO (blue) and NO occupancy in the presence of O_2 (Salmon). Hydrogen bonds were identified by using the cut-off distance of 3.5 Å between hydrogen bond donor/acceptor atoms and a bond angle cut-off of 120°. The concentrations of mitoNEET were (A, C) 16 μM or (E) 19 μM. The ratio of $(S_2O_4)^{2-}$, DEA NONOate (NO donor), H_2S donor or pioglitazone to mitoNEET was 1. All experiments were repeated at least three times to confirm reproducibility. Buffer was phosphate 50 mM, 100 mM NaCl, pH 7. (A, C, E) Samples were prepared at room temperature (~ 22 °C).

using pioglitazone (Fig. 5B and Fig. S7F) showed that this ligand also binds to the surface of mitoNEET and interacts with Val70, Pro100, Leu101 and Ile102, the residues forming the NO entry site. Therefore, pioglitazone may block the NO access and thereby prevent the reaction of NO with the mitoNEET [2Fe-2S] cluster. To test this possibility, we added pioglitazone to mitoNEET (1 : 1 ratio) before (Fig. 5C) or after (Fig. S7G) exposure to NO under abnormally low O_2 levels (5 ppm). mitoNEET was incubated with the NO-donor reagent. After overnight incubation to ensure the removal of NO gas from the solution, H_2S donor was added. We observed that under these conditions, H_2S was able to reduce the cluster (Fig. 5C), unlike in the absence of pioglitazone (Fig. 5A). Therefore, pioglitazone blocked the NO diffusion towards the cluster and thereby preventing the cluster desensitization towards reduction by H_2S.

O_2 blocks NO access

The link between hypoxia and mitochondrial dysfunction is established [44,64], and mitoNEET oxidation state is linked to voltage gating function of VDAC1

and mitochondrial function [25]. Additionally, hypoxia affects mitochondrial [Fe-S] cluster biogenesis and causes VDAC1 cleavage [65]. However, it is unknown if normoxic conditions would protect the mitoNEET [2Fe-2S] cluster against NO oxidation and desensitization towards reduction by H_2S. To this end, we first studied how the O_2 level would affect the mitoNEET cellular level. Interferons do not induce the expression of mitoNEET. Therefore, we compared the mitoNEET cellular level with an O_2-sensitive [Fe-S] enzyme, namely, Elp3, whose expression is not induced by interferons. Additionally, Elp3 has the same [4Fe-4S](Cys)$_3$ cluster as interferon-stimulated hSAND. We tested if the levels of mitoNEET and Elp3 in effector T cells (T_{effs}) were affected by hypoxic conditions (Fig. 5D). We chose these T cells because their function and activity in diseases such as cancer is regulated by hypoxia and NO [66,67]. While the hypoxic condition significantly increased the cellular level of Elp3, it did not substantially affect that of mitoNEET (Fig. 5D). These results suggest that under low O_2 levels, the [4Fe-4S] cluster is less degraded, stabilizing the protein and increasing its level, but the mitoNEET [2Fe-2S] cluster was not affected as expected from our biochemical data showing O_2 resistance at pH 7.0. Next, we studied if a high O_2 level (21% O_2, approximately 254 μM) can protect mitoNEET [2Fe-2S] cluster against NO desensitization toward H_2S reduction. To perform this experiment, we first confirm that under our experimental condition, at a mitoNEET and NO-donor (DEA NONOate) concentration of 16 μM used for NO/O_2 competition studies (Fig. 5E), NO is released throughout circa 4 h and the reaction of NO with O_2 is negligible. The mass conservation equation (Data S1) predicts an NO release rate of less than 0.1 μM·s^{-1}, at which the reaction of NO with O_2 is negligible (Fig. S8A,B). This release rate and the availability of NO for approximately 4 h under aerobic conditions were further confirmed using spin-trap experiments (Fig. S8C–E). We then exposed mitoNEET to NO under normoxic conditions (O_2 level 254 μM), and after 4 h to remove almost all NO, mitoNEET was treated with H_2S donor under anaerobic conditions. We found that H_2S reduced the cluster (Fig. 5E), unlike when mitoNEET was exposed to NO in the presence of very low amount of O_2 (Fig. 5A). Therefore, high O_2 levels protect the [2Fe-2S] cluster against NO reaction and desensitization towards H_2S reduction. To understand how O_2 could block NO reaction with the cluster, we performed MD simulations in a mixture of O_2/NO. We sampled the NO or O_2 interactions with mitoNEET (Data S1). The average backbone RMSD values of the protein for 50 ns were below 2 Å (Fig. S9A), indicating that the system is in thermal equilibrium and stable. Interaction studies revealed that O_2 forms hydrogen bonds with residues at the interface between two subunits, namely, Tyr71 and Arg73, and that the NO ability to form hydrogen bonds with these residues is abolished (Fig. 5F). This effect of O_2 on NO interaction is similar to that we observed for V70W mutation (Fig. 3E). Additionally, the O_2 survival probability remains near 100% after 20 ns compared to the survival probability of NO, which decreases (Fig. S9B). These predictions suggest that O_2 blocks NO access to the cluster. Exposure of the reduced V70W or V70C variant to O_2 led to the formation of oxidized protein (Fig. S9C,D). Therefore, it appears that O_2 access to the cluster is not solely dependent on the NO access tunnel. Blocking NO access will possibly facilitate the auto-oxidation of NO by O_2 before it reaches the cluster.

Discussion

Previous works with mitoNEET focused on the individual reaction of O_2, NO or H_2O_2 with its [2Fe-2S] cluster, but the mechanism of the reaction at the molecular level, the competition between NO and O_2 and the reaction of H_2S with the cluster were not studied [31,33–40,55]. It was shown that the half-life of mitoNEET [2Fe-2S] cluster under aerobic conditions increased exponentially by increasing pH from circa 5 to 6.7 [31,36,37]. Decreasing pH to less than 7, a pH value less than the pKa of histidine ligand of the mitoNEET [2Fe-2S] cluster, makes the cluster labile and unstable [33,34]. The pH-dependent liability of the cluster explains why, at low pH, the cluster is not stable in the presence of O_2. Therefore, it is expected that at pH 7 or above, the mitoNEET cluster is oxygen resistant. Consistently, we found that in phosphate buffer with a pH value of 7.0, the cluster is highly resistant to O_2 degradation. Similarly, at pH 7, the mitoNEET [2Fe-2S] cluster is stable in response to H_2O_2 exposure and is not degraded [31,37,38], consistent with our findings. Adding 500 μM H_2O_2 after reducing the cluster with DTT (10 000 μM) was suggested to oxidize the cluster transiently [35]. When we added H_2O_2 in the absence of sodium dithionite, we observed that the cluster was stable, and the reduced mitoNEET [2Fe-2S]$^{1+}$ cluster was oxidized. Finally, under anaerobic conditions, NO oxidizes the cluster of the NEET family of proteins and binds to the cluster to generate iron-nitrosyl species [38–40,55]. Similarly, we observed that NO oxidizes and interacts with the mitoNEET [2Fe-2S] cluster under anaerobic conditions, generating iron-nitrosyl species.

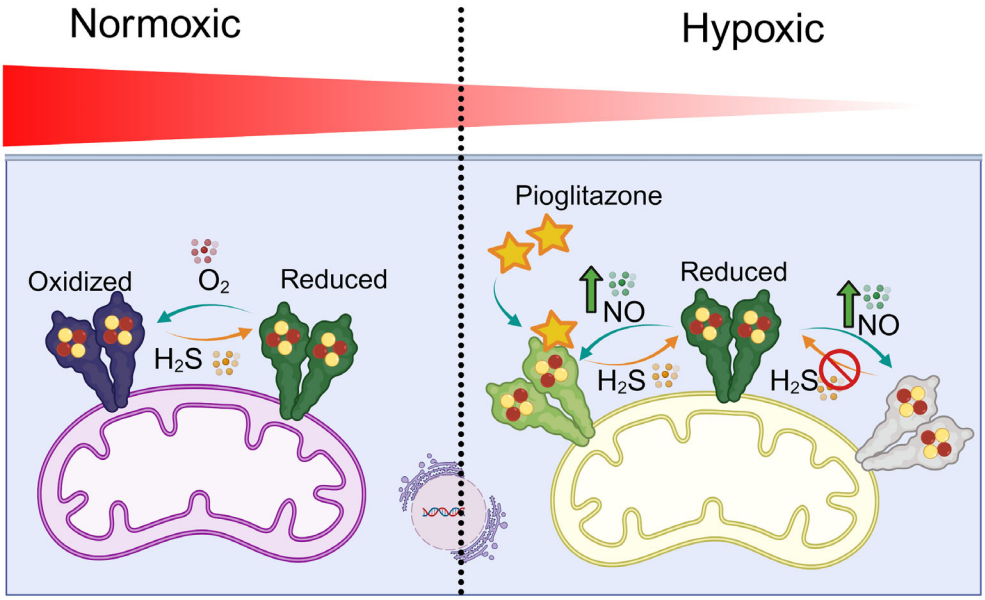

Fig. 6. A schematic model describing the molecular function of mitoNEET [2Fe-2S] cluster in sensing O_2 level and gasotransmitters. Under normoxic conditions, O_2 protects the mitoNEET [2Fe-2S] cluster (left). Under inflammatory and hypoxic conditions (right), when the NO level rises, mitoNEET is oxidized by NO and desensitized to H_2S reduction (grey). Pioglitazone protects the mitoNEET cluster against NO oxidation and enables H_2S reduction (light greeen).

Unlike previous reports, here we studied the molecular mechanism of the reaction of O_2 and gasotransmitters NO and H_2S with mitoNEET [2Fe-2S] cluster and investigated how the presence of O_2 affects these reactions. We first combined MD simulations and mutagenesis studies to elucidate the NO pathway to the cluster. We discovered an explicit NO access tunnel. We showed for the first time that gasotransmitter H_2S can reduce the mitoNEET [2Fe-2S] cluster. Based on these findings, we tested whether the O_2 level affects NO oxidation and H_2S reduction. When the O_2 level was very low, exposure of mitoNEET to NO led to the desensitization of the cluster towards H_2S reduction. However, under normoxic conditions or when pioglitazone was added, NO access to the cluster was blocked and the cluster was not desensitized towards reduction by H_2S. These data together confirm the presence of an O_2-regulated NO access site to the mitoNEET [2Fe-2S] cluster. These findings also suggest a new biological action of H_2S. The reaction of gasotransmitter H_2S with [Fe-S] proteins, including the NEET family, and its interplay with oxidizing signalling molecules like NO and O_2 have not been studied previously. H_2S has multiple functions [68]. It can coordinate with metallocofactors in haemoglobin, reduce disulphide bonds, oxidize radicals like NO and superoxide and form covalent bonds with amino acid residues of proteins [68]. Our data suggest that H_2S can reduce certain [Fe-S] clusters.

Based on our findings, we put forward a molecular mechanism for the interplay among NO, O_2 and H_2S reactions with mitoNEET [2Fe-2S] cluster (Fig. 6). Under hypoxic and inflammatory conditions characterized by an increase and a decrease in the NO and O_2 levels, respectively, there will be an increase in the reaction of NO with mitoNEET [2Fe-2S] cluster. The NO reaction desensitizes the oxidized mitoNEET $[2Fe\text{-}2S]^{2+}$ cluster towards reduction by biological reductants like gasotransmitter H_2S or other biologically relevant reducing agents, for example, anamorsin/Ndor1 complex [69]. As a result, the concentration of the NO-oxidized and -desensitized mitoNEET rises. The presence of pioglitazone restores the balance between the reduced and oxidized mitoNEET. It is known that the redox state of mitoNEET plays an essential role in mitochondrial oxidative capacity and function [23,24]. The oxidized mitoNEET interacts with VDAC [23], reducing mitochondrial membrane potential. A reduction in mitoNEET expression level enhances mitochondrial respiration [25], and mitoNEET knockout mice show signs of mitochondrial dysfunction and a Parkinson's disease phenotype [27]. While mitoNEET loss leads to mitochondrial dysfunction in B-cell acute lymphoblastic leukaemia [28], its activity reduces oxidative damage to conserve mitochondrial function [63].

Consequently, based on our findings and model (Fig. 6), we postulate that under hypoxic conditions, an increase in NO-desensitized mitoNEET contributes to the loss of mitochondrial membrane potential and the formation of dysfunctional mitochondria. By blocking NO access to the cluster, pioglitazone restores the balance between oxidized and reduced mitoNEET, attenuating oxidative damage and restoring mitochondrial function/integrity [29]. Future cell-based experiments should test the link between our model and the function of mitoNEET in modulating mitochondrial activity.

In conclusion, we discovered an explicit NO access site to the mitoNEET [2Fe-2S] cluster, suggesting a molecular mechanism of mitoNEET function in gasotransmitter signal transduction. Our data collectively revealed that O_2 and, similarly, pioglitazone block the NO access and protect the mitoNEET [2Fe-2S] cluster from NO desensitization. These findings will have broad implications for understanding the pathways *via* which hypoxia affects mitochondrial function and designing new therapeutics to target mitoNEET.

Acknowledgements

TNH acknowledges support from the Vietnamese Government Scholarship. KHE and TNH are grateful to King's College London for an International Student Fee Waiver Grant. KHE thanks the Royal Society for an International Exchanges Grant (IES\R1\221117) and a Research Grant (RGS\R1\231135). KHE, SK and MH acknowledge support from MRC Doctoral Network Program. EPR studies at TU Delft were supported by a COST Action CA21115 Short-Term Scientific Mission Grant to TNH. MMR thanks the EPSRC (grant EP/W005794/1) for funding. The EPR measurements were performed at the Centre for Pulse EPR at Imperial College London (PEPR), supported by the EPSRC grant EP/T031425/1 to MMR. Computational studies were funded by the German Research Foundation (DFG) under Germany's Excellence Strategy – EXC 2008-390540038 – UniSysCat to MAM. This article is based on work from COST Action FeS-ImmChemNet (CA21115) supported by COST (European Cooperation in Science and Technology).

Author contributions

KHE conceived the project; TNH performed all biochemical measurements; MW-L carried out computational studies; AC and P-LH performed EPR measurements; MA and MH carried out experiments with T cells and performed western blot measurements; TNH and KHE designed experiments; all authors contributed to the discussion and analyses of data; TNH and KHE prepared the manuscript draft with contribution from all authors; TNH, SK, P-LH, MAM, MMR and KHE received funding.

Data accessibility

The data, excluding EPR and computational data, that support the findings of this study are openly available on Dryad at https://doi.org/10.5061/dryad.3xsj3txrz, reference number FEBSL-24-1135. The EPR and computational data that support the findings of this study are available on request from the corresponding author, as they are not publicly available due to privacy.

References

1 Ebrahimi KH, Ciofi-Baffoni S, Hagedoorn P-L, Nicolet Y, Le Brun NE, Hagen WR and Armstrong FA (2022) Iron–sulphur clusters as inhibitors and catalysts of viral replication. *Nat Chem* **14**, 253–266.
2 Braymer JJ, Freibert SA, Rakwalska-Bange M and Lill R (2021) Mechanistic concepts of iron–sulfur protein biogenesis in biology. *Biochim Biophys Acta Mol Cell Res* **1868**, 118863.
3 Maio N and Rouault TA (2015) Iron–sulfur cluster biogenesis in mammalian cells: new insights into the molecular mechanisms of cluster delivery. *Biochim Biophys Acta Mol Cell Res* **1853**, 1493–1512.
4 Garcia PS, D'Angelo F, Ollagnier de Choudens S, Dussouchaud M, Bouveret E, Gribaldo S and Barras F (2022) An early origin of iron–sulfur cluster biosynthesis machineries before earth oxygenation. *Nat Ecol Evol* **6**, 1564–1572.
5 Lill R (2009) Function and biogenesis of iron–sulphur proteins. *Nature* **460**, 831–838.
6 Rouault TA (2015) Mammalian iron–sulphur proteins: novel insights into biogenesis and function. *Nat Rev Mol Cell Biol* **16**, 45–55.
7 Bridges HR, Fedor JG, Blaza JN, di Luca A, Jussupow A, Jarman OD, Wright JJ, Agip ANA, Gamiz-Hernandez AP, Roessler MM *et al.* (2020) Structure of inhibitor-bound mammalian complex I. *Nat Commun* **11**, 5261.
8 Zhu J, Vinothkumar KR and Hirst J (2016) Structure of mammalian respiratory complex I. *Nature* **536**, 354–358.
9 Amara P, Saragaglia C, Mouesca J-M, Martin L and Nicolet Y (2022) L-tyrosine-bound ThiH structure reveals C–C bond break differences within radical SAM aromatic amino acid lyases. *Nat Commun* **13**, 2284.
10 Johnson DC, Dean DR, Smith AD and Johnson MK (2005) Structure, function, and formation of biological iron–sulfur clusters. *Annu Rev Biochem* **74**, 247–281.

11 Crack JC, Green J, Thomson AJ and Le Brun NE (2014) Iron–sulfur clusters as biological sensors: the chemistry of reactions with molecular oxygen and nitric oxide. *Acc Chem Res* **47**, 3196–3205.
12 SantaMaria AM and Rouault TA (2024) Regulatory and sensing iron–sulfur clusters: new insights and unanswered questions. *Inorganics* **12**, 101.
13 Crack JC and Le Brun N (2024) Binding of a single nitric oxide molecule is sufficient to disrupt DNA binding of the nitrosative stress regulator NsrR. *Chem Sci* **15**, 18920–18932.
14 Crack JC and Le Brun NE (2021) Biological iron–sulfur clusters: mechanistic insights from mass spectrometry. *Coord Chem Rev* **448**, 214171.
15 Nechushtai R, Karmi O, Zuo K, Marjault HB, Darash-Yahana M, Sohn YS, King SD, Zandalinas SI, Carloni P and Mittler R (2020) The balancing act of NEET proteins: iron, ROS, calcium and metabolism. *Biochim Biophys Acta Mol Cell Res* **1867**, 118805.
16 Nicolet Y (2020) Structure–function relationships of radical SAM enzymes. *Nat Catal* **3**, 337–350.
17 Landgraf BJ, McCarthy EL and Booker SJ (2016) Radical S-adenosylmethionine enzymes in human health and disease. *Annu Rev Biochem* **85**, 485–514.
18 Ji Y, Wei L, Da A, Stark H, Hagedoorn P-L, Ciofi-Baffoni S, Cowley SA, Louro RO, Todorovic S, Mroginski MA *et al.* (2022) Radical-SAM dependent nucleotide dehydratase (SAND), rectification of the names of an ancient iron–sulfur enzyme using NC-IUBMB recommendations. *Front Mol Biosci* **19**, 1032220.
19 Ebrahimi KH, Gilbert-Jaramillo J, James WS and McCullagh JSO (2021) Interferon-stimulated gene products as regulators of central carbon metabolism. *FEBS J* **288**, 3715–3726.
20 Hoang TN, Shahmohammadi S and Ebrahimi KH (2023) Ancient complexes of iron and sulfur modulate oncogenes and oncometabolism. *Curr Opin Chem Biol* **76**, 102338.
21 Camponeschi F, Piccioli M and Banci L (2022) The intriguing mitoNEET: functional and spectroscopic properties of a unique [2Fe-2S] cluster coordination geometry. *Molecules* **27**, 8218.
22 Geldenhuys WJ, Leeper TC and Carroll RT (2014) mitoNEET as a novel drug target for mitochondrial dysfunction. *Drug Discov Today* **19**, 1601–1606.
23 Lipper CH, Stofleth JT, Bai F, Sohn YS, Roy S, Mittler R, Nechushtai R, Onuchic JN and Jennings PA (2019) Redox-dependent gating of VDAC by mitoNEET. *Proc Natl Acad Sci U S A* **116**, 19924–19929.
24 Wiley SE, Murphy AN, Ross SA, van der Geer P and Dixon JE (2007) MitoNEET is an iron-containing outer mitochondrial membrane protein that regulates oxidative capacity. *Proc Natl Acad Sci U S A* **104**, 5318–5323.
25 Kusminski CM, Holland WL, Sun K, Park J, Spurgin SB, Lin Y, Askew GR, Simcox JA, McClain DA, Li C *et al.* (2012) MitoNEET-driven alterations in adipocyte mitochondrial activity reveal a crucial adaptive process that preserves insulin sensitivity in obesity. *Nat Med* **18**, 1539–1549.
26 Furihata T, Takada S, Kakutani N, Maekawa S, Tsuda M, Matsumoto J, Mizushima W, Fukushima A, Yokota T, Enzan N *et al.* (2021) Cardiac-specific loss of mitoNEET expression is linked with age-related heart failure. *Commun Biol* **4**, 138.
27 Geldenhuys WJ, Benkovic SA, Lin L, Yonutas HM, Crish SD, Sullivan PG, Darvesh AS, Brown CM and Richardson JR (2017) MitoNEET (CISD1) knockout mice show signs of striatal mitochondrial dysfunction and a Parkinson's disease phenotype. *ACS Chem Nerosci* **8**, 2759–2765.
28 Geldenhuys WJ, Piktel D, Moore JC, Rellick SL, Meadows E, Pinti MV, Hollander JM, Ammer AG, Martin KH and Gibson LF (2021) Loss of the redox mitochondrial protein mitoNEET leads to mitochondrial dysfunction in B-cell acute lymphoblastic leukemia. *Free Radic Biol Med* **175**, 226–235.
29 Yonutas HM, Hubbard WB, Pandya JD, Vekaria HJ, Geldenhuys WJ and Sullivan PG (2020) Bioenergetic restoration and neuroprotection after therapeutic targeting of mitoNEET: new mechanism of pioglitazone following traumatic brain injury. *Exp Neurol* **327**, 113243.
30 Bai F, Morcos F, Sohn YS, Darash-Yahana M, Rezende CO, Lipper CH, Paddock ML, Song L, Luo Y, Holt SH *et al.* (2015) The Fe-S cluster-containing NEET proteins mitoNEET and NAF-1 as chemotherapeutic targets in breast cancer. *Proc Natl Acad Sci U S A* **112**, 3698–3703.
31 Mons C, Botzanowski T, Nikolaev A, Hellwig P, Cianférani S, Lescop E, Bouton C and Golinelli-Cohen MP (2018) The H_2O_2-resistant Fe–S redox switch MitoNEET acts as a pH sensor to repair stress-damaged Fe–S protein. *Biochemistry* **57**, 5616–5628.
32 Zuris JA, Harir Y, Conlan AR, Shvartsman M, Michaeli D, Tamir S, Paddock ML, Onuchic JN, Mittler R, Cabantchik ZI *et al.* (2011) Facile transfer of [2Fe-2S] clusters from the diabetes drug target mitoNEET to an apo-acceptor protein. *Proc Natl Acad Sci U S A* **108**, 13047–13052.
33 Wiley SE, Paddock ML, Abresch EC, Gross L, van der Geer P, Nechushtai R, Murphy AN, Jennings PA and Dixon JE (2007) The outer mitochondrial membrane protein mitoNEET contains a novel redox-active 2Fe-2S cluster. *J Biol Chem* **282**, 23745–23749.
34 Bak DW and Elliott SJ (2013) Conserved hydrogen bonding networks of MitoNEET tune Fe-S cluster

binding and structural stability. *Biochemistry* **52**, 4687–4696.
35 Landry AP and Ding H (2014) Redox control of human mitochondrial outer membrane protein MitoNEET [2Fe-2S] clusters by biological thiols and hydrogen peroxide. *J Biol Chem* **289**, 4307–4315.
36 Golinelli-Cohen M-P, Lescop E, Mons C, Gonçalves S, Clémancey M, Santolini J, Guittet E, Blondin G, Latour JM and Bouton C (2016) Redox control of the human iron-sulfur repair protein MitoNEET activity via its iron-sulfur cluster. *J Biol Chem* **291**, 7583–7593.
37 Salameh M, Riquier S, Guittet O, Huang ME, Vernis L, Lepoivre M and Golinelli-Cohen MP (2021) New insights of the NEET protein CISD2 reveals distinct features compared to its close mitochondrial homolog mitoNEET. *Biomedicine* **9**, 384.
38 Grifagni D, Silva JM, Querci L, Lepoivre M, Vallières C, Louro RO, Banci L, Piccioli M, Golinelli-Cohen MP and Cantini F (2024) Biochemical and cellular characterization of the CISD3 protein: molecular bases of cluster release and destabilizing effects of nitric oxide. *J Biol Chem* **300**, 105745.
39 Fontenot CR, Cheng Z and Ding H (2022) Nitric oxide reversibly binds the reduced [2Fe-2S] cluster in mitochondrial outer membrane protein mitoNEET and inhibits its electron transfer activity. *Front Mol Biosci* **9**, 995421.
40 Cheng Z, Landry AP, Wang Y and Ding H (2017) Binding of nitric oxide in CDGSH-type [2Fe-2S] clusters of the human mitochondrial protein Miner2. *J Biol Chem* **292**, 3146–3153.
41 Pappas G, Wilkinson ML and Gow AJ (2023) Nitric oxide regulation of cellular metabolism: adaptive tuning of cellular energy. *Nitric Oxide* **131**, 8–17.
42 Murphy B, Bhattacharya R and Mukherjee P (2019) Hydrogen sulfide signaling in mitochondria and disease. *FASEB J* **33**, 13098–13125.
43 Solaini G, Baracca A, Lenaz G and Sgarbi G (2010) Hypoxia and mitochondrial oxidative metabolism. *Biochim Biophys Acta* **1797**, 1171–1177.
44 Mialet-Perez J and Belaidi E (2024) Interplay between hypoxia inducible factor-1 and mitochondria in cardiac diseases. *Free Radic Biol Med* **221**, 13–22.
45 Alharbi AF, Kim H, Chumroo D, Ji Y, Hakil M and Ebrahimi KH (2023) VITAS, a sensitive in vivo selection assay to discover enzymes producing antiviral natural products. *Chem Commun* **59**, 5419–5422.
46 Salmon DJ, Torres de Holding CL, Thomas L, Peterson KV, Goodman GP, Saavedra JE, Srinivasan A, Davies KM, Keefer LK and Miranda KM (2011) HNO and NO release from a primary amine-based Diazeniumdiolate as a function of pH. *Inorg Chem* **50**, 3262–3270.
47 Ramamurthi A and Lewis RS (1997) Measurement and modeling of nitric oxide release rates for nitric oxide donors. *Chem Res Toxicol* **10**, 408–413.
48 Xing W, Yin M, Lv Q, Hu Y, Liu C and Zhang J (2014) 1 – Oxygen solubility, diffusion coefficient, and solution viscosity. In Rotating Electrode Methods and Oxygen Reduction Electrocatalysts (Xing W, Yin G and Zhang JB, eds), pp. 1–31. Elsevier, Amsterdam. doi: 10.1016/B978-0-444-63278-4.00001-X
49 Gizzi AS, Grove TL, Arnold JJ, Jose J, Jangra RK, Garforth SJ, du Q, Cahill SM, Dulyaninova NG, Love JD *et al.* (2018) A naturally occurring antiviral ribonucleotide encoded by the human genome. *Nature* **558**, 610–614.
50 Ebrahimi KH, Vowles J, Browne C, McCullagh J and James WS (2020) ddhCTP produced by the radical-SAM activity of RSAD2 (viperin) inhibits the NAD+-dependent activity of enzymes to modulate metabolism. *FEBS Lett* **594**, 1631–1644.
51 Ebrahimi KH, Silveira C and Todorovic S (2018) Evidence for the synthesis of an unusual high spin ($S = 7/2$) [Cu–3Fe–4S] cluster in the radical-SAM enzyme RSAD2 (viperin). *Chem Commun* **54**, 8614–8617.
52 Pokidova OV, Novikova VO, Emel'yanova NS, Kormukhina AY, Kulikov AV, Utenyshev AN, Lazarenko VA, Ovanesyan NS, Starostina AA and Sanina NA (2023) A nitrosyl iron complex with 3.4-dichlorothiophenolyl ligands: synthesis, structures and its reactions with targets–carriers of nitrogen oxide (NO) in vivo. *Dalton Trans* **52**, 2641–2662.
53 Crack JC, Hamilton CJ and Le Brun N (2018) Mass spectrometric detection of iron nitrosyls, sulfide oxidation and mycothiolation during nitrosylation of the NO sensor [4Fe–4S] NsrR. *Chem Commun* **54**, 5992–5995.
54 Miranda KM (2005) The chemistry of nitroxyl (HNO) and implications in biology. *Coord Chem Rev* **249**, 433–455.
55 Wang Y, Lee J and Ding H (2019) Light-induced release of nitric oxide from the nitric oxide-bound CDGSH-type [2Fe–2S] clusters in mitochondrial protein Miner2. *Nitric Oxide* **89**, 96–103.
56 Lewandowska H, Kalinowska M, Brzóska K, Wójciuk K, Wójciuk G and Kruszewski M (2011) Nitrosyl iron complexes—synthesis, structure and biology. *Dalton Trans* **40**, 8273–8289.
57 Tinberg CE, Tonzetich ZJ, Wang H, Do LH, Yoda Y, Cramer SP and Lippard SJ (2010) Characterization of iron Dinitrosyl species formed in the reaction of nitric oxide with a biological Rieske center. *J Am Chem Soc* **132**, 18168–18176.
58 Kabil O, Motl N and Banerjee R (2014) H_2S and its role in redox signaling. *Biochim Biophys Acta* **1844**, 1355–1366.
59 Zuris JA, Paddock ML, Abresch EC, Conlan AR, Nechushtai R and Jennings PA (2009) Redox potential of the outer-mitochondrial membrane 2Fe-2S protein MitoNEET. *Biophys J* **96**, 240a.

60 Dicus MM, Conlan A, Nechushtai R, Jennings PA, Paddock ML, Britt RD and Stoll S (2010) Binding of histidine in the (Cys) 3 (his) 1-coordinated [2Fe-2S] cluster of human mitoNEET. *J Am Chem Soc* **132**, 2037–2049.
61 Iwasaki T, Samoilova RI, Kounosu A, Ohmori D and Dikanov SA (2009) Continuous-wave and pulsed EPR characterization of the [2Fe-2S](Cys) 3 (his) 1 cluster in rat MitoNEET. *J Am Chem Soc* **131**, 13659–13667.
62 Hammack CD, Perry G, LeBaron RG, Villareal G and Phelix CF (2015) Low dose pioglitazone attenuates oxidative damage in early Alzheimer's disease by binding mitoNEET: transcriptome-to-Reactome™ biosimulation of neurons. *Int J Knowl Discov Bioinforma* **5**, 24–45.
63 Tam E and Sweeney G (2024) MitoNEET provides Cardioprotection via reducing oxidative damage and conserving mitochondrial function. *Int J Mol Sci* **25**, 480.
64 Scharping NE, Rivadeneira DB, Menk AV, Vignali PDA, Ford BR, Rittenhouse NL, Peralta R, Wang Y, Wang Y, DePeaux K *et al*. (2021) Mitochondrial stress induced by continuous stimulation under hypoxia rapidly drives T cell exhaustion. *Nat Immunol* **22**, 205–215.
65 Ferecatu I, Canal F, Fabbri L, Mazure NM, Bouton C and Golinelli-Cohen MP (2018) Dysfunction in the mitochondrial Fe-S assembly machinery leads to formation of the chemoresistant truncated VDAC1 isoform without HIF-1α activation. *PLoS One* **13**, e0194782.
66 Vignali PDA, DePeaux K, Watson MLJ, Ye C, Ford BR, Lontos K, McGaa NK, Scharping NE, Menk AV, Robson SC *et al*. (2023) Hypoxia drives CD39-dependent suppressor function in exhausted T cells to limit antitumor immunity. *Nat Immunol* **24**, 267–279.
67 García-Ortiz A and Serrador JM (2018) Nitric oxide signaling in T cell-mediated immunity. *Trends Mol Med* **24**, 412–427.
68 Szabó C (2007) Hydrogen sulphide and its therapeutic potential. *Nat Rev Drug Discov* **6**, 917–935.
69 Camponeschi F, Ciofi-Baffoni S and Banci L (2017) Anamorsin/Ndor1 complex reduces [2Fe–2S]-MitoNEET via a transient protein–protein interaction. *J Am Chem Soc* **139**, 9479–9482.

Supporting information

Additional supporting information may be found online in the Supporting Information section at the end of the article.

Data S1. Supplementary methods.
Fig. S1. Degradation of hSAND cluster by O_2, H_2O_2 and NO.
Fig. S2. The O_2, H_2O_2 and NO reaction with mitoNEET [2Fe-2S] cluster.
Fig. S3. Evaluation of protein stability and prediction of gas tunnels and a gas gate in mitoNEET.
Fig. S4. V70C mutation does not affect NO interaction with residues near the [2Fe-2S] cluster.
Fig. S5. The mutation of valine 70 to tryptophane (V70W) or to cysteine (V70C) does not affect the [2Fe-2S] cluster.
Fig. S6. H_2S reaction with hSAND and mitoNEET.
Fig. S7. Pioglitazone protects the mitoNEET [2Fe-2S] cluster from NO reaction.
Fig. S8. NO release rate and availability in the presence of O_2.
Fig. S9. MD simulations of mix NO and O_2 diffusion in mitoNEET.
Table S1. MitoNEET residues with C-α located in a 3.5 Å radius of the [2Fe-2S] cluster establish contact with H_2O_2 and NO molecules (diffusant).
Table S2. List of mitoNEET residues that participate in Tunnel 1 and those that are involved in the entry site to the tunnel, according to predictions from the CAVER WEB 1.0 server.